NASA TECHNICAL MEMORANDUM

NASA TM X-2309

NASA TM X-2309

LIFT INDUCED ON A SWEPT WING BY A TWO-DIMENSIONAL PARTIAL-SPAN DEFLECTED JET AT MACH NUMBERS FROM 0.20 TO 1.30

by Blake W. Corson, Jr., Francis J. Capone, and Lawrence E. Putnam

Langley Research Center
Hampton, Va. 23365

NATIONAL AERONAUTICS AND SPACE ADMINISTRATION • WASHINGTON, D. C. • AUGUST 1971

1. Report No.	2. Government Accession No.	3. Recipient's Catalog No.
NASA TM X-2309		

4. Title and Subtitle	5. Report Date
LIFT INDUCED ON A SWEPT WING BY A TWO-DIMENSIONAL PARTIAL-SPAN DEFLECTED JET AT MACH NUMBERS FROM 0.20 TO 1.30	August 1971
	6. Performing Organization Code

7. Author(s)	8. Performing Organization Report No.
Blake W. Corson, Jr., Francis J. Capone, and Lawrence E. Putnam	L-7707
	10. Work Unit No.
9. Performing Organization Name and Address	764-74-02-01
NASA Langley Research Center Hampton, Va. 23365	11. Contract or Grant No.
	13. Type of Report and Period Covered
12. Sponsoring Agency Name and Address	Technical Memorandum
National Aeronautics and Space Administration Washington, D.C. 20546	14. Sponsoring Agency Code

15. Supplementary Notes

16. Abstract

An exploratory investigation has been conducted in the Langley 16-foot transonic tunnel at Mach numbers from 0.20 to 1.30 to determine the induced lift characteristics of a body and swept-wing configuration having a partial-span two-dimensional propulsive nozzle with exhaust exit in the notch of the swept-wing trailing edge. The effects on wing-body characteristics of deflecting the propulsive jet in the flap mode at nominal exhaust-nozzle deflection angles from 0° to 30° have been studied. The Reynolds number based on wing mean geometric chord varied from 1.35×10^{6} to 3.86×10^{6}.

17. Key Words (Suggested by Author(s))	18. Distribution Statement
Jet flap Induced lift Subsonic Transonic	Unclassified – Unlimited

19. Security Classif. (of this report)	20. Security Classif. (of this page)	21. No. of Pages	22. Price*
Unclassified	Unclassified	65	$3.00

*For sale by the National Technical Information Service, Springfield, Virginia 22151

LIFT INDUCED ON A SWEPT WING BY A TWO-DIMENSIONAL PARTIAL-SPAN DEFLECTED JET AT MACH NUMBERS FROM 0.20 TO 1.30

By Blake W. Corson, Jr., Francis J. Capone,
and Lawrence E. Putnam
Langley Research Center

SUMMARY

An exploratory investigation has been conducted in the Langley 16-foot transonic tunnel at Mach numbers from 0.20 to 1.30 to determine the induced lift characteristics of a body and swept-wing configuration having a partial-span two-dimensional propulsive nozzle with exhaust exit in the notch of the swept-wing trailing edge. The Reynolds number based on wing mean geometric chord varied from 1.35×10^6 to 3.86×10^6. The effects on wing-body characteristics of deflecting the propulsive jet in the flap mode at nominal exhaust-nozzle deflection angles from 0^o to 30^o have been studied.

Results of the investigation indicated that deflecting the jet induced a flow field which resulted in an increase in lift by an amount up to three times the magnitude of the lift component of the exhaust-nozzle gross thrust. At subsonic speeds, the body-alone configuration developed about one-half as much induced lift as developed on the wing and body combined. The induced flow field created by the deflected jet reacts with the wing and body to reduce drag by an amount of about 3 percent of the nozzle ideal gross thrust at a Mach number of 0.90 at the higher jet deflection angles.

INTRODUCTION

The design of high-speed V/STOL aircraft is usually complicated by such deficiencies as excessive weight, requirement for special lift engines, complexity of mechanical or gas ducting systems, and severe trim changes related to the lift augmentation. For example, requirement for special lift engines can be accompanied by an increase in frontal area and decrease in fineness ratio which usually results in an increase in drag at transonic and supersonic speeds.

In an attempt to alleviate some of the deficiencies associated with high-speed V/STOL aircraft, a research program has been initiated to develop a high-speed aircraft configuration having STOL properties and a highly sweptback wing with a jet flap located

in the wing trailing-edge notch. The span of the jet flap would be much less than the wing span. This configuration would be powered with centrally located turbojet or turbofan engines. The deflected jet would serve two purposes: (1) to obtain an increase in lift at cruise conditions due to the induced flow field associated with the deflected jet with possibly no increase in cruise drag and (2) to produce additional lift as a result of being used as a transonic maneuver device. The experimental results presented herein were obtained in an exploratory investigation of the foregoing concept which was conducted as much as possible with existing hardware. Consequently, the model configuration was not intended to represent a practical aircraft configuration. This investigation was conducted in the Langley 16-foot transonic tunnel over a Mach number range from 0.20 to 1.30 and at Reynolds numbers based on the mean geometric chord ranging from 1.35×10^6 to 3.86×10^6.

The jet-flap concept is based on the premise that the spanwise dimension of the propulsive exhaust jet is several times greater than the jet thickness and that the exhaust nozzles are articulated so that the exhaust jet may be deflected in the mode of a trailing-edge flap. The conceptual partial-span jet flap permits the use of all the engine exhaust to simulate the jet flap, avoids ducting through the wing, and limits mechanical articulation to the exhaust nozzles (and possibly to wing leading-edge flaps).

A sweptback wing has two possible advantages. One advantage is that certain sweptback wings can be designed to have the aerodynamic center close to the trailing-edge notch. With exhaust jets deflected in this vicinity, the jet gross thrust vector lies close to the moment center and, consequently, does not produce large changes in pitching moment when the direction of the jet thrust vector is varied. A second advantage is improved lift augmentation when the jet is deflected. If, in a very elementary sense, the induced flow field of an isolated lifting flap or jet flap is regarded as similar to that induced by a horseshoe vortex, the net induced velocities within the horseshoe vortex are negative and those outside the vortex are positive, that is in the lift direction. When the deflected jet flap is located in the trailing-edge notch of a swept wing, the net induced velocities tend only to increase the wing lift. Having the outboard panels of the wing swept back places this portion of the wing in a stronger upwash than if the wing were not swept and tends to compensate for the short span of the jet flap.

Analytical studies of the foregoing concept, using the methods of references 1 and 2, indicated that for a plane wing at zero angle of attack, the lift induced on the wing by the deflected jet flap would be about three times the magnitude of the lift component of the exhaust-nozzle gross thrust.

SYMBOLS

Model forces and moments are referred to a stability-axis system with the model moment reference center at the intersection of the body center line and the nozzle exit plane, which corresponds to the 0.517 wing-mean-geometric-chord location.

A_e exhaust nozzle exit area

A_{gap} model total cross-sectional area at metric break at station 52.07, 182.41 cm^2

AR wing aspect ratio, 2.47

C_D drag coefficient, $\frac{D}{qS}$

$C_{D,net}$ net drag coefficient (see eq. (7))

$C_{(F-D)}$ coefficient of resultant axial force, $\frac{F_{AX}}{qS}$

C_L lift coefficient, $\frac{L}{qS}$

$(C_L)_{C_T=0}$ jet-off lift coefficient

$C_{L,j}$ coefficient of jet thrust component in lift direction, $\frac{F_g \sin(\delta + \alpha)}{qS}$

$C_{L,s}$ static lift coefficient, $\frac{N}{qS}$

$C_{L,\Gamma}$ coefficient of jet-circulation lift

C_m pitching-moment coefficient, $\frac{\text{Pitching moment}}{qS\bar{c}}$

C_T nozzle gross thrust coefficient, $\frac{F_g}{qS}$

$C_{T,i}$ ideal isentropic gross thrust coefficient, $\frac{F_i}{qS}$

$C_{T,i,s}$ static ideal isentropic gross thrust coefficient, $\frac{F_i}{p_\infty S}$

$C_{T,s}$ static coefficient of resultant axial force, $\frac{F_{AX}}{p_\infty S}$

$\bar{c}$	wing mean geometric chord, 27.51 cm
D	drag in streamwise direction
e	span efficiency factor
F	thrust component parallel to body longitudinal axis, positive toward nose, $F_g \cos \delta$
$F_{A,bal}$	axial force measured by balance including gap pressure force, positive toward nose
F_{AX}	resultant axial force parallel to body axis, positive toward nose
F_g	nozzle gross thrust parallel to nozzle axis, ηF_i
F_i	ideal isentropic nozzle gross thrust parallel to nozzle axis
G	gain factor (see eq. (2))
i_w	wing angle of incidence
L	lift normal to relative wind and spanwise axis
M	Mach number
$\dot{m}$	measured mass-flow rate
$\dot{m}_i$	ideal mass-flow rate
N	normal force or static lift normal to body longitudinal and spanwise axes, positive toward top of airframe
$\bar{p}_{gap}$	average static pressure acting on body metric break
$p_{t,j}$	jet total pressure
p_∞	free-stream or ambient static pressure

q	free-stream dynamic pressure
R	gas constant (for $\gamma = 1.4$), 287.3 N-m/kg-K
S	wing reference area, 1554.81 cm^2
$T_{t,j}$	jet total temperature
α	body angle of attack
γ	ratio of specific heats, 1.40 for air
Δ	increment or finite difference
δ	effective jet deflection angle (see eq. (3))
δ_d	design or nominal nozzle deflection angle, angle between body longitudinal axis and nozzle geometric axis in plane of symmetry
η	nozzle thrust ratio, $\frac{F_g}{F_i}$

APPARATUS AND PROCEDURE

Exhaust-Nozzle Simulation System

A sketch of the strut-supported jet-engine exhaust-nozzle simulation system used in the present investigation is presented as figure 1. The body consisted of a conical forebody with a 14° half-angle and a 15.24-centimeter-diameter cylindrical centerbody to which various exhaust nozzles can be attached at station 104.14. The forebody was supported from the tunnel floor by a fixed strut having a 45° leading-edge sweep and a 5-percent-thick (streamwise) hexagonal airfoil. The body center line is 91.40 centimeters below the wind-tunnel center line.

A continuous flow of dry high-pressure air at approximately 300 K was used to simulate the jet exhaust. The air is introduced perpendicularly to the model axis into the section of the model supported by the force balance through eight sonic nozzles equally spaced around a center core to eliminate transfer of axial momentum. Two flexible metal bellows, arranged so that one is ahead and one is behind the respective points of attachments to the fixed portion of the model, seal the forward portion of the low-pressure air chamber; this arrangement prevents the pressurizing of the bellows

from loading the balance. The flow-straightening screens were made of 0.635-mesh, 0.0635-centimeter-diameter wire cloth supported by a coarse grid of streamlined vanes.

Only that portion of the configuration aft of the metric break at station 52.07 is supported by the force balance and hereinafter is referred to as the wind-tunnel model.

Model

The overall planform of the model is presented in figure 2. Photographs of the model are shown as figure 3. Details of the wing and nozzles are presented in figures 4 and 5, respectively. An existing axisymmetric afterbody, attached at station 104.14 and terminated at station 121.92, was modified so that wings and nozzle inserts of varying deflection angles could be attached. Initially a wing planform was chosen so that the quarter-chord of the wing mean geometric chord would be located at the jet exit in order to minimize large changes in pitching moment with operation of the jet at deflected conditions. However, from structural considerations necessary for attaching the existing wing panels, the requirement to have the wing aerodynamic center at the nozzle exit was relaxed. The nozzle exit was fixed at station 127.00.

The midwing used in this investigation had a leading-edge sweep of 66.88°, a trailing-edge sweep of 32.00°, and an NACA 63A008 airfoil section that was parallel to the actual tip chord. The wing reference area was 1554.8 centimeters^2 and included the crosshatched area indicated in figure 2. The wing had a mean geometric chord of 27.51 centimeters, a span of 61.98 centimeters, and an aspect ratio of 2.47 based on the wing reference area. Provision was made to vary wing incidence angle from -2.26° to 0.62°.

The nozzle aspect ratio (width to depth ratio) was approximately 3.40 for all nozzles and the values of the exit areas are tabulated in figure 5. Seven nozzle inserts were provided; they were attached at station 121.92 and had design deflection angles from 0° to 30°.

Transforming the flow from axisymmetric to two-dimensional and turning the flow were both accomplished internally. Because of limitations imposed by the wing attachment, these nozzles had an unusually large boattail angle of 36.29°. The wing trailing edge at its intersection with the undeflected nozzle was fixed at the nacelle center line. Thus, as jet deflection angle increases, there is both a rotation and a translation of the nozzle exit with respect to the wing trailing edge, as indicated in figure 5.

Wind Tunnel and Instrumentation

This investigation was conducted in the Langley 16-foot transonic tunnel which is a single-return atmospheric wind tunnel with slotted octagonal test section and continuous

air exchange. The wind tunnel has continuously variable airspeed up to a Mach number of 1.30. Test-section plenum suction is used for speeds above a Mach number of 1.10. From calibrations of the wind tunnel, the test-section-wall divergence is adjusted as a function of airstream dew point in order to eliminate any longitudinal static-pressure gradients in the test section that might occur due to condensation of atmospheric moisture.

Aerodynamic forces were measured with an internal three-component strain-gage balance. Internal static pressure at the metric break at station 52.07 was determined by measurement of the pressure at 12 locations in the vicinity of the break by using individual pressure transducers. These pressure measurements are used to adjust the measured balance forces for the force acting across the break station to a free-stream static pressure. Total pressure of the jet flow was measured with two pressure transducers; the total-pressure probes, indicated in figure 1, were located at model stations 95.00 and 96.52 at meridian angles of 340° and 160°, respectively. Total temperatures of the jet flow were measured with two iron-constantan thermocouples located at model stations 95.76 and 97.28 at meridian angles of 250° and 70°, respectively. A turbine flowmeter was used to obtain mass-flow rate to the nozzle.

At each test point, approximately 10 frames of data were recorded on magnetic tape over a period of about 5 seconds as Mach number and jet total-pressure ratio were held constant; the average value of these 10 recordings were used for computational purposes.

Tests

Seven nozzles with design jet deflection angles δ_d of 0°, 5°, 10°, 15°, 20°, 25°, and 30° were tested at Mach numbers from 0 to 0.98 at a wing incidence angle of -1.38°. Some additional tests were conducted with the 0° and 30° nozzles at Mach numbers from 0 to 1.30. These tests were made with a wing-off configuration and wing-on configurations at incidence angles of -2.26°, -1.38°, and 0.62°. Reynolds number based on the wing mean geometric chord varied from 1.35×10^6 to 3.86×10^6. Balance load limit on pitching moment restricted the maximum obtainable jet pressure ratio for the nozzles with the larger deflection angles.

All tests were conducted with 0.25-centimeter-wide boundary-layer transition strips consisting of No. 100 silicon carbide grit sparsely distributed in a thin film of lacquer. These strips were located 2.54 centimeters from the tip of the forebody nose and on both the upper and lower surfaces of the wings at 10 percent of the local streamwise chord.

DATA ANALYSIS

Basic Forces, Gain Factor, and Jet Deflection Angle

In the present investigation the body and balance longitudinal axes were at all times coincident and parallel to the free airstream. Body angle of attack was always zero, but wing incidence was varied through a small angle range as has been noted.

The lift measured by the force balance is composed of three parts expressed in coefficient form as follows:

$$C_L = (C_L)_{C_T=0} + C_{L,\Gamma} + C_T \sin(\delta + \alpha) \tag{1}$$

Since $\alpha = 0^\circ$,

$$C_L = (C_L)_{C_T=0} + C_{L,\Gamma} + C_T \sin \delta$$

where $(C_L)_{C_T=0}$ is the jet-off lift coefficient of the model, $C_T \sin \delta$ is the component of nozzle gross thrust in the lift direction, and $C_{L,\Gamma}$ is the coefficient of lift on the wing and body induced by the deflected jet, which is defined in reference 3 as the jet-circulation lift coefficient.

The gain factor is defined as

$$G = \frac{C_{L,\Gamma} + C_T \sin \delta}{C_T \sin \delta} \tag{2}$$

The numerator of equation (2) is determined by subtracting the jet-off lift coefficient from the total lift coefficient measured with the jet operating. In applying equation (2) in the present investigation, for simplicity C_T in the denominator was replaced by $C_{T,i}$ which makes the values of gain factor presented in the figures conservative by as much as 4 percent at high jet total-pressure ratio.

Because forces were measured with a single balance, the balance reading indicates net force – that is, the sum of forces exerted by the external airstream and jet reaction forces. Therefore, only at static conditions (M = 0), when the external aerodynamic forces are assumed to be zero, can the effective jet deflection angle δ be measured. The jet deflection angle is defined as

$$\delta = \arctan \frac{N}{F} \tag{3}$$

where N and F are normal and axial forces at static conditions. Figure 6 presents the static data for the various nozzles as a function of jet total-pressure ratio. In determining the gain factor, it is assumed that the measured effective jet deflection angle δ is a characteristic of the nozzle internal geometry and does not vary with Mach number.

The ideal isentropic gross thrust or exhaust jet momentum is defined as

$$F_i = \dot{m}\sqrt{RT_{t,j}}\sqrt{\left(\frac{2\gamma}{\gamma - 1}\right)\left[1 - \left(\frac{p_\infty}{p_{t,j}}\right)^{\frac{\gamma-1}{\gamma}}\right]} \tag{4}$$

where $\dot{m}$ is the measured mass-flow rate and $p_{t,j}$ is the corrected average jet total pressure. A total-pressure rake was used to survey the jet-total-pressure distribution at the exit of the nozzles, and the average jet-total-pressure probe readings were corrected to the integrated value of jet total pressure at the exit. This correction to account for flow nonuniformity was approximately 1.2 percent for the nozzles having design deflection angles of 0^o and 30^o, and this correction was applied to all the nozzles. The variation of nozzle ideal isentropic gross thrust coefficient, measured mass-flow rate, and discharge coefficient with jet total-pressure ratio for selected nozzles is shown in figure 7.

The coefficient of resultant axial force $C_{(F-D)}$ is obtained by adjusting the measured balance axial force for the gap pressure force as follows:

$$F_{AX} = \left[F_{A,bal} + \left(\bar{p}_{gap} - p_\infty\right)A_{gap}\right]$$

$$F_{AX} = F_g \cos\delta + L \sin\alpha - D\cos\alpha$$

In the present investigation, $\alpha = 0^o$ and

$$F_{AX} = \left(F_g \cos\delta - D\right) = (F - D) \tag{5}$$

$$C_{(F-D)} = \frac{F_{AX}}{qS} \tag{6}$$

For static operation (M = 0), drag is assumed to be zero and

$$F_{AX} = F = F_g \cos\delta$$

$$C_{T,S} = \frac{F_{AX}}{p_\infty S}$$

Thrust Recovery

When the model angle of attack is zero and the jet is deflected at an angle δ, a loss of thrust along the body axis proportional to $1 - \cos \delta$ is anticipated. However, the deflected jet does increase circulation about the wing and alters the flow field surrounding the model. If this altered flow field induced by the deflected jet results in increased wing leading-edge suction or reduced afterbody drag, these beneficial effects may be regarded as thrust recovery.

A thrust recovery parameter is defined in reference 3 as

$$\text{Thrust recovery} = \frac{C_{D,net}}{-C_{T,i}}$$

where

$$C_{D,net} = C_D - (C_D)_{C_T=0} - \frac{(C_{L,\Gamma})^2}{e\pi AR} \tag{7}$$

However, in the present investigation the last term in equation (7) could not be determined because the angle-of-attack range for the wing was limited to small changes in incidence angle, and the angle of attack of the model remained at zero. From equation (5), the resultant axial force is

$$F_{AX} = (F - D) = F_g \cos \delta - D$$

$$(F - D) = \eta F_i \cos \delta - D$$

where $\eta = \frac{F_g}{F_i}$. The drag of the model then can be expressed as

$$D = \eta F_i \cos \delta - (F - D)$$

Dividing by qS yields

$$C_D = \eta C_{T,i} \cos \delta - C_{(F-D)}$$

and differentiating with respect to $C_{T,i}$ then gives

$$\frac{dC_D}{dC_{T,i}} = \frac{d(\eta C_{T,i} \cos \delta)}{dC_{T,i}} - \frac{dC_{(F-D)}}{dC_{T,i}} \tag{8}$$

The left-hand side of equation (8) may be expressed as finite differences, where ΔD is a change in model drag and corresponds to a finite change in ideal thrust ΔF_i and where in application ΔF_i will be taken as the change from zero ideal thrust, that is,

$$\Delta F_i = F_i - 0 = F_i$$

This procedure is valid for functions which are generally linear within the interval of application, such as those in figure 8. Thus,

$$\frac{dC_D}{dC_{T,i}} = \frac{\Delta D}{\Delta F_i} = \frac{\Delta D}{F_i}$$

The foregoing relation which expresses a change in drag of the model as a fraction of ideal thrust when substituted in equation (8) yields

$$\frac{\Delta D}{F_i} = \frac{d\left(\eta C_{T,i} \cos \delta\right)}{dC_{T,i}} - \frac{dC_{(F-D)}}{dC_{T,i}} \tag{9}$$

The form of equation (9) has been chosen to permit evaluation of changes in model drag, expressed as a fraction of ideal thrust, by use of measured slopes of data plots. In the first term on the right of equation (9), η and δ are to be treated as constants so that

$$\frac{d\left(\eta C_{T,i} \cos \delta\right)}{dC_{T,i}} = \eta \cos \delta$$

$$\frac{\Delta D}{F_i} = \left(\eta \cos \delta - \frac{dC_{(F-D)}}{dC_{T,i}}\right) \tag{10}$$

Equation (10) expresses a change in model drag related to changing ideal thrust from zero to F_i. The point of real interest is the magnitude of the change in this force increment when the jet deflection angle is changed from zero to a finite value. In this investigation, the thrust recovery factor is defined as

$$\frac{\Delta F}{F_i} = \left(\frac{\Delta D}{F_i}\right)_{\delta=0} - \left(\frac{\Delta D}{F_i}\right)_{\delta} \tag{11}$$

Figure 6(a) shows that for a nominal jet deflection angle of 0^o, the measured deflection was sufficiently small to regard $\cos \delta$ as unity. The thrust recovery factor then is

$$\frac{\Delta F}{F_i} = \left(\eta - \frac{dC_{(F-D)}}{dC_{T,i}}\right)_{\delta=0} - \left(\eta \cos \delta - \frac{dC_{(F-D)}}{dC_{T,i}}\right)_{\delta} \tag{12}$$

Because values of the nozzle internal performance η are only slightly less than unity and are assumed not to change with jet deflection angle, equation (12) is simplified by assuming $\eta = 1.0$. Thus,

$$\frac{\Delta F}{F_i} = \left(1 - \frac{dC_{(F-D)}}{dC_{T,i}}\right)_{\delta=0} - \left(\cos \delta - \frac{dC_{(F-D)}}{dC_{T,i}}\right)_{\delta} \tag{13}$$

$$\frac{\Delta F}{F_i} = \left[\left(\frac{dC_{(F-D)}}{dC_{T,i}}\right)_{\delta} - \left(\frac{dC_{(F-D)}}{dC_{T,i}}\right)\right]_{\delta=0} + (1 - \cos \delta) \tag{14}$$

The values of thrust recovery factor presented in the figures were computed by use of equation (14).

PRESENTATION OF RESULTS

The results of this investigation are presented in the following figures:

DISCUSSION

Lift Augmentation Characteristics

The effects on the basic aerodynamic characteristics of varying nozzle deflection angle from 0^o to 30^o are shown in figure 8. It is noted that the combination of increasing the ideal gross thrust coefficient (except at $\delta_d = 0^o$) and jet deflection angle increases

the total lift of the configuration throughout the Mach number range. This increase in lift above the jet-off value is the sum of the component of the thrust vector in the lift direction $C_{L,j}$ and the induced or jet-circulation lift $C_{L,\Gamma}$.

The jet-off lift has been subtracted from the lift data of figure 8 and the resultant $C_{L,j} + C_{L,\Gamma}$ (jet lift plus jet-circulation lift) data are presented in figure 9 as a function of measured nozzle deflection angle for constant values of ideal gross thrust coefficient. The resultant $C_{L,j} + C_{L,\Gamma}$ data are nearly linear with δ up to $M = 0.40$ with the curves becoming more nonlinear as Mach number increases. Two-dimensional results of reference 4 show that this lift has a linear variation with $\sin \delta$ up to deflection angles of about 60°. Figure 10 presents the variation of jet-circulation lift with ideal gross thrust coefficient; these values were obtained by subtracting the computed values of the jet lift $\left(C_{T,i} \sin \delta\right)$ from the data of figure 9. These values tend to be conservative since the computed ideal gross thrust is used and does not take into account the nozzle internal frictional losses.

The variation of the gain factor G (obtained from eq. (2)) with ideal gross thrust coefficient for various exhaust-nozzle deflection angles at a wing incidence angle of -1.38° is presented in figure 11. The gain factor decreases with increasing ideal thrust coefficient and for the larger deflection angles (generally at or above 15°) increases with increasing deflection angle except at $M = 0.20$ and 0.40 where the apparent scatter in the gain factor for the smaller deflection angles is probably due to accuracy limitations in measuring small values of lift by the force balance. The maximum value of G was 3.15 for $\delta_d = 30^{\circ}$, $M = 0.80$, and $i_w = -1.38^{\circ}$. The increase in the gain factor with increasing deflection angle is consistent with the three-dimensional jet-flap results summarized in reference 1; whereas, two-dimensional results tend to show that the gain factor is independent of deflection angle.

Some limited tests were conducted in order to determine the effects of wings off and wing incidence angle on gain factor at a jet deflection angle of 30°. The results of these tests are summarized in figure 12. The gain factor increased as wing incidence angle increased at all Mach numbers. A maximum gain factor value of 3.95 was achieved at $M = 0.70$ for $C_{T,i} = 0.036$. The basic data for these configurations (not shown) are similar to those presented in figure 8 except the jet-off values of C_L and C_m are different depending on wing incidence angle. At subsonic speeds, the body-alone configuration developed about one-half as much induced lift as developed on the wing and body combined. This result may indicate that further increases in induced lift may be possible by properly shaping the aircraft fuselage immediately forward of the jet exit. However, care must also be exercised in any shaping of the fuselage to insure that afterbody boattail drag is kept as small as possible. A configuration employing a two-dimensional jet flap as described in the introduction might have steeper boattail angles than a comparable configuration with two or more circular jet exits.

Comparisons are made in figure 13 of gain factors from the present investigation at $M = 0.20$, 0.40, and 0.70 for $\delta_d = 30^\circ$ and $i_w = -1.38^\circ$ with two-dimensional theoretical and empirically determined gain factors and some results of other investigations. The theory of reference 5 assumes an infinitely thin jet issuing at small deflection angles. However, since comparisons of theoretical data with experimental data in reference 5 at deflection angles up to 58.1° show good agreement up to $C_{T,i} = 2.0$, theoretical gain factors for $\delta = 70^\circ$ have been presented where it is assumed that these values would be in agreement with experimental results. The empirical results of reference 6 were based on two-dimensional tests where $C_{L,\Gamma} + C_{L,j}$ was found to be proportional to $\sqrt{C_{T,i}}$ and $\sin \delta$ (up to about 65°). The constant of proportionality is given in reference 6 for three cases: (1) the pure jet flap, (2) blowing symmetrically over a deflected flap, and (3) blowing only over the upper surface of the flap. Gain factors for only the first and third cases are presented in figure 13.

On the basis of the results presented in figure 13, some qualitative observations on the relative performance of the configuration of the present investigation can be made. The results of reference 4 for a jet flap on a delta wing with leading-edge sweep of 60°, $\delta = 70^\circ$, and $M = 0.30$ show a reduction of about 62 percent in gain factor when compared with the two-dimensional theory for $\delta = 70^\circ$. Reference 4 estimated that $C_{L,\Gamma} + C_{L,j} = 1.46 \sin \delta \sqrt{C_{T,i}}$. The lower value of the gain factor is probably attributed to three-dimensional effects and reduced induced lift due to the low-aspect-ratio wing. (See ref. 1 for summary of some aspect-ratio effects.) For the present investigation, an average reduction in gain factor of about 78 percent occurred over a $C_{T,i}$ range from 0.06 to 0.10 at $M = 0.70$. This further reduction in induced lift (as compared with the results of ref. 4) is caused primarily by (1) the partial-span jet flap and (2) the jet thickness. Most jet-flap tests have been conducted with very narrow slots where the ratio of slot thickness to wing mean geometric chord varied from 0.003 to 0.02 because the original jet-flap concept called for a jet sheet to issue from the wing (ref. 1). However, the ratio of slot thickness to wing mean geometric chord was 0.1 for the present investigation.

Some insight into expected reduction in gain factor due to the partial-span jet and three-dimensional effects may be seen by first comparing three-dimensional experimental blown flap data (blowing over upper surface of a wing flap) of reference 6 with the two-dimensional empirical results, also of reference 6. A reduction in gain factor of 64 percent at $C_{T,i} = 0.4$ and 76 percent at $C_{T,i} = 1.0$ occurred. These values compare with reductions in gain factor of 75 percent and 68 percent for the present test.

Although these results tend to show poorer performance in lift augmentation when compared with other results, it must be remembered that this concept of a jet flap

involved deflection of the aircraft exhaust nozzles in order to avoid ducting of hot gases through the wing and, thus, departed from classic jet-flap design.

Pitching-Moment Characteristics

Positive increases in pitching moment occurred as ideal gross thrust coefficient was increased at all Mach numbers except $M = 0.98$ for nozzle deflection angles greater than 10°. (See fig. 8.) At a deflection angle of 5°, generally there was a slight decrease in pitching moment at the lower values of ideal thrust coefficient and a slight increase at the higher values. The nose-up pitching moment is due principally to the induced lift acting forward of the moment reference center since the exhaust-nozzle thrust vector was designed to act through this moment reference center.

The nose-down pitching moments that usually result from deflecting the jet can probably be trimmed by use of a canard. This design feature depends on the extent of V/STOL operation required. A canard would require a positive up load which would increase the overall lift coefficient of the aircraft configuration. This would be beneficial for an aircraft engaged in air-to-air combat at high subsonic speeds where high lift is essential provided that wing buffet does not occur (ref. 7). An aircraft configuration with a jet flap should also have a higher buffet onset envelope since results of tests made with a two-dimensional jet-flap wing at high subsonic speeds (refs. 8 and 9) showed that the lift coefficient for buffet onset increased with blowing over the flap.

Thrust Recovery

Theoretically, for the two-dimensional jet-flap wing the sum of the streamwise component of thrust plus thrust recovery equals the jet reaction regardless of the jet deflection angle (refs. 1 and 10). However, as pointed out in reference 3, the entrainment of the surrounding air by the deflected jet causes a deviation from potential theory. Reference 3 also assumes that thrust recoveries somewhere between the component in the thrust direction (jet at some deflection angle) and full jet reaction (no deflection angle) could be obtained. Accordingly, in reference 3 a thrust recovery parameter in terms of a net drag coefficient was defined (eq. (7)) and thrust recovery was shown to occur.

However, as stated in the section entitled "DATA ANALYSIS" such a parameter is not possible to obtain for the present investigation and a thrust recovery parameter was defined (eq. (14)) in terms of the ideal thrust based on the linear portion of the thrust-minus-drag curves. These results are presented in figure 14 and show thrust recovery to increase with increasing jet deflection angle at most Mach numbers. This trend is similar to that shown in reference 3. At $M = 0.90$ and $\delta_d = 30^{\circ}$, approximately 3 percent of the deflected ideal thrust vector $\left(C_{T,i} \cos \delta\right)$ is recovered.

CONCLUSIONS

An exploratory investigation has been conducted in the Langley 16-foot transonic tunnel at Mach numbers from 0.20 to 1.30 to determine the induced lift characteristics of a body and swept-wing configuration having a partial-span two-dimensional propulsive nozzle with exhaust exit in the notch of the swept-wing trailing edge. The Reynolds number based on wing mean geometric chord varied from 1.35×10^6 to 3.86×10^6. Investigation of the effects on wing-body characteristics of deflecting the propulsive jet in the flap mode at nominal exhaust-nozzle deflection angles from 0^o to 30^o leads to the following conclusions:

1. Deflecting the jet induced a flow field which resulted in an increase in lift by an amount up to three times the magnitude of the lift component of the exhaust-nozzle gross thrust.

2. At subsonic speeds, the body-alone configuration developed about one-half as much induced lift as developed on the wing and body combined.

3. The induced flow field created by the deflected jet reacts with the wing and body to reduce drag by an amount of about 3 percent of the nozzle ideal gross thrust at a Mach number of 0.90 at the higher jet deflection angles.

Langley Research Center,
National Aeronautics and Space Administration,
Hampton, Virginia, June 29, 1971.

REFERENCES

1. Korbacher, G. K.; and Sridhar, K.: A Review of the Jet Flap. UTIA Rev. No. 14, Inst. Aerophys., Univ. of Toronto, May 1960.

2. Lamar, John E.: A Modified Multhopp Approach for Predicting Lifting Pressures and Camber Shape for Composite Planforms in Subsonic Flow. NASA TN D-4427, 1968.

3. Lowry, John G.; Riebe, John M.; and Campbell, John P.: The Jet-Augmented Flap. Preprint No. 715, S.M.F. Fund Paper, Inst. Aeronaut. Sci., Jan. 1957.

4. Malavard, L.; Poisson-Quinton, Ph.; and Jousserandot, P.: Recherches Théoriques et Expérimentales Sur le Contrôle de Circulation Par Soufflage Appliqué aux Ailes D'Avions. O.N.E.R.A. Note Tech. No. 37, 1956.

5. Spence, D. A.: The Lift Coefficient of a Thin, Jet-Flapped Wing. Proc. Roy. Soc. (London), ser. A, vol. 238, no. 1212, Dec. 4, 1956, pp. 46-68.

6. Poisson-Quinton, Ph.; and Lepage, L.: Survey of French Research on the Control of Boundary Layer and Circulation. Boundary Layer and Flow Control, Vol. I, G. V. Lachmann, ed., Pergamon Press, Inc., 1961, pp. 21-73.

7. Ray, Edward J.; and Taylor, Robert T.: Buffet and Static Aerodynamic Characteristics of a Systematic Series of Wings Determined From a Subsonic Wind-Tunnel Study. NASA TN D-5805, 1970.

8. Grahame, W. E.; Headley, J. W.; and Rogers, L. W.: Recent Experience in the Transonic Testing of Two-Dimensional Swept and Straight Wings With High Lift Devices. Facilities and Techniques for Aerodynamic Testing at Transonic Speeds and High Reynolds Number, AGARD Conf. Pre-Print No. 83, Apr. 1971, 6-1–6-17.

9. Peake, D. J.; Yoshihara, H.; Zonars, D; and Carter, W.: The Transonic Performance of Two-Dimensional, Jet-Flapped Aerofoils at High Reynolds Numbers. Presented at the AGARD Specialists' Meeting on Facilities and Techniques for Aerodynamic Testing at Transonic Speeds and High Reynolds Numbers (Göttingen, Ger.), Apr. 26-28, 1971.

10. Davidson, I. M.: The Jet Flap. J. Roy. Aeronaut. Soc., vol. 60, no. 541, Jan. 1956, pp. 25-50.

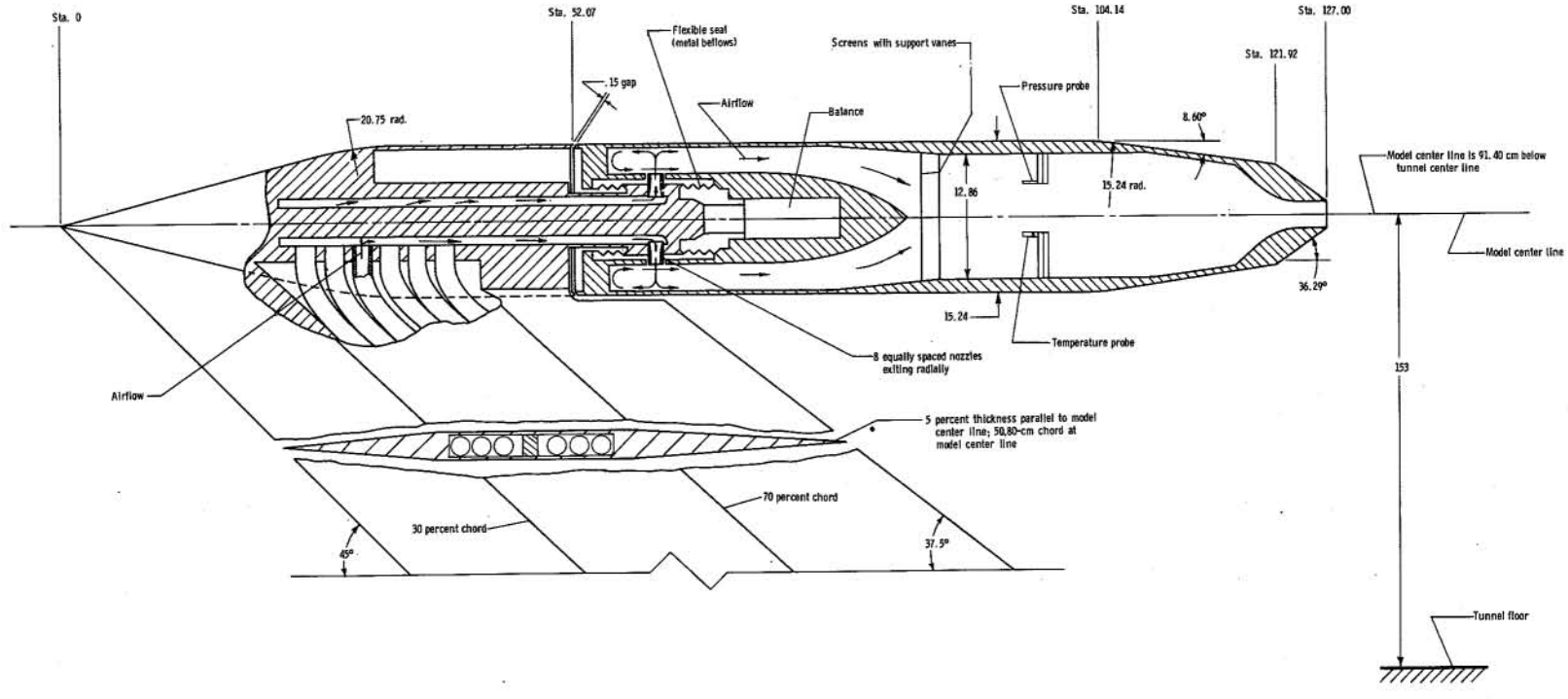

Figure 1.- Simplified sketch of jet-engine exhaust-nozzle simulator. $\delta_d = 0^o$.
All dimensions are in centimeters unless otherwise noted.

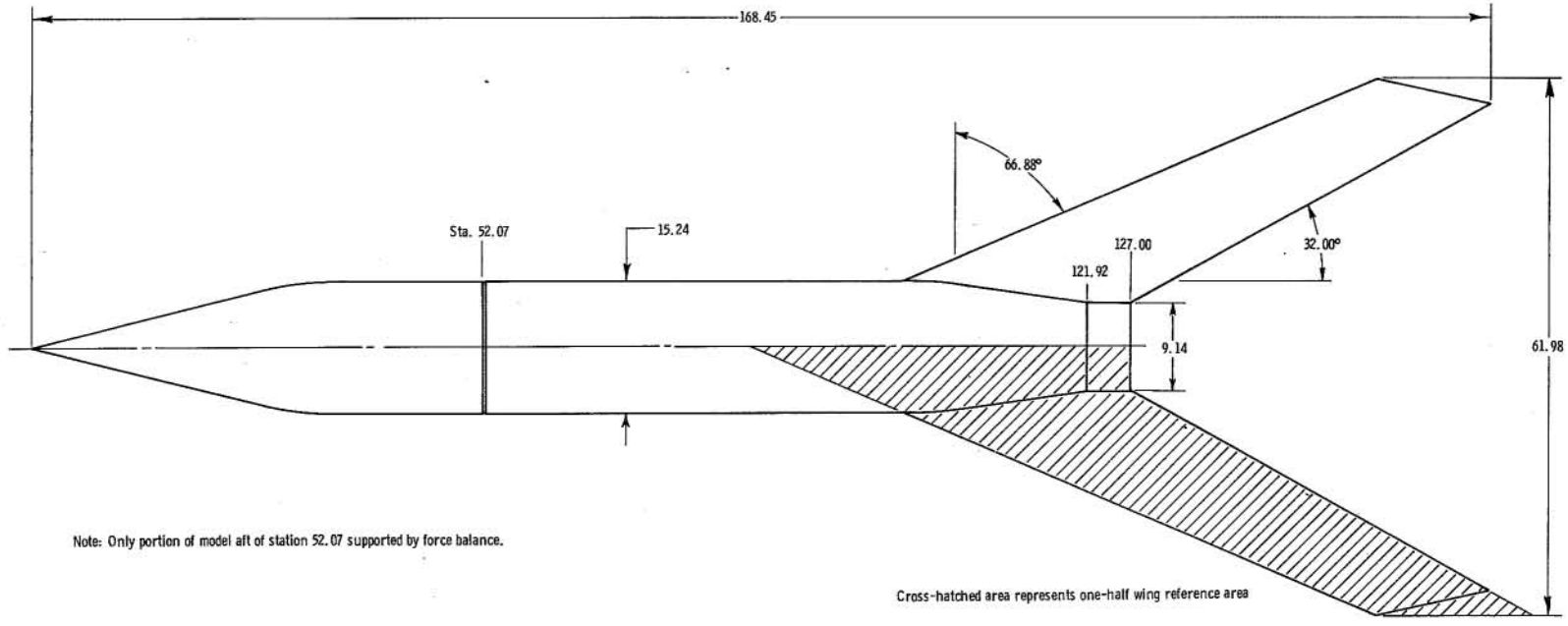

Figure 2.- Overall planform of model. All dimensions are in centimeters unless otherwise noted.

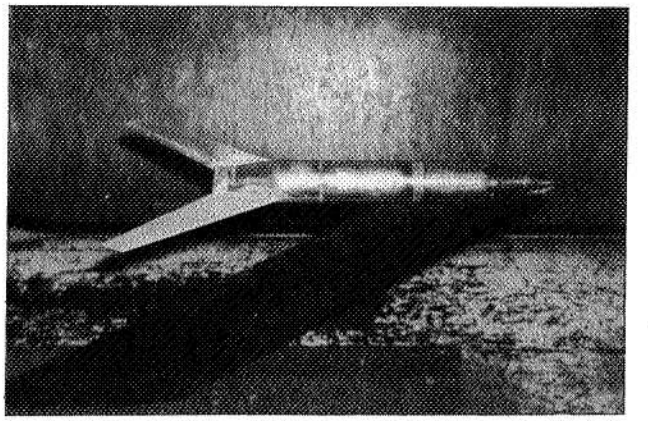

(a) Overall view with $\delta_d = 0^o$.

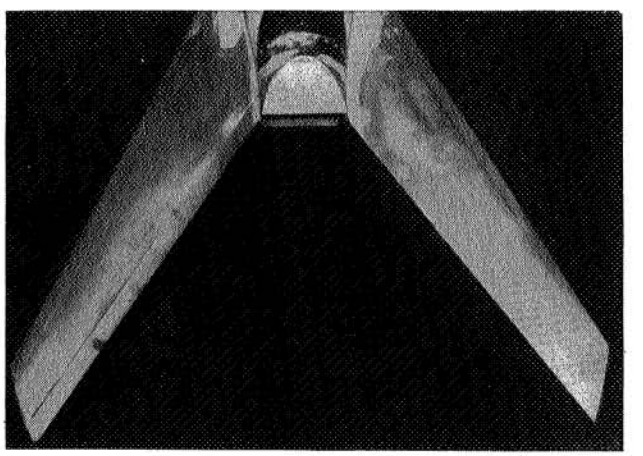

(b) Top view with $\delta_d = 0^o$.

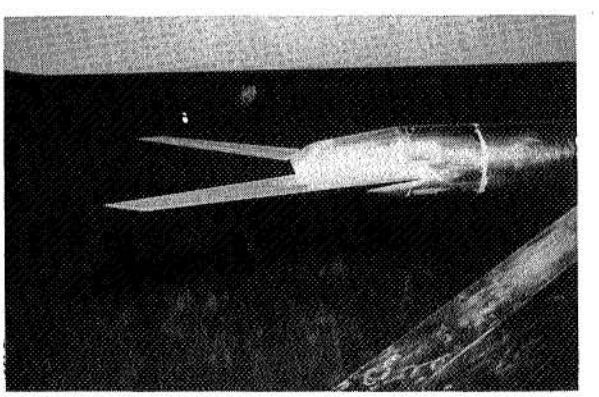

L-71-642

(c) Side view with $\delta_d = 30^o$.

Figure 3.- Photographs of model.

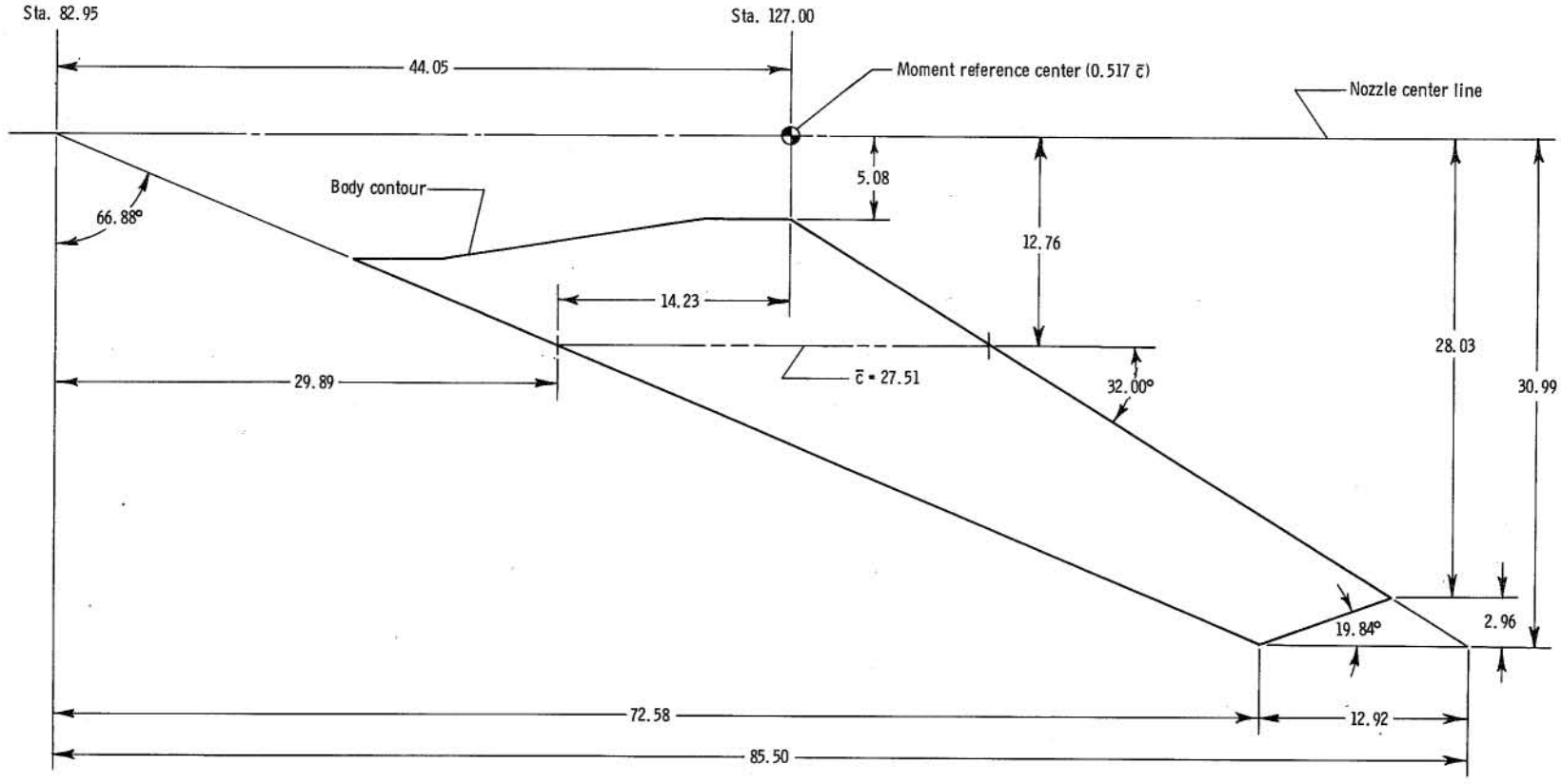

Figure 4.- Wing geometry. All dimensions are in centimeters unless otherwise noted.

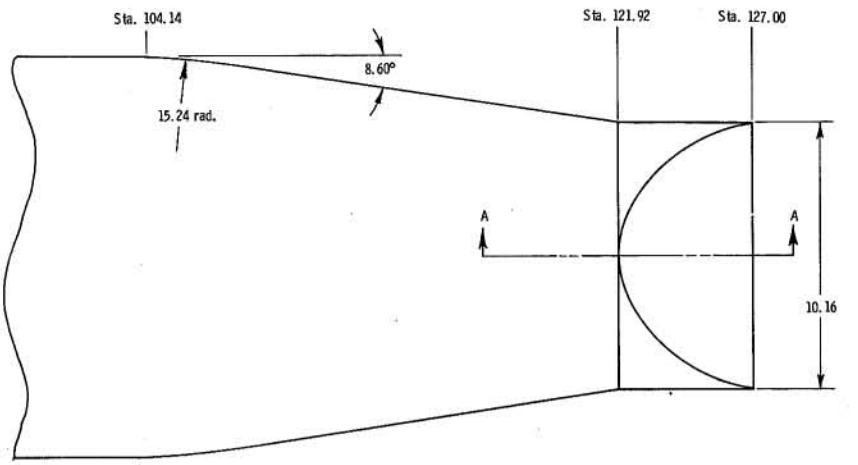

Top view

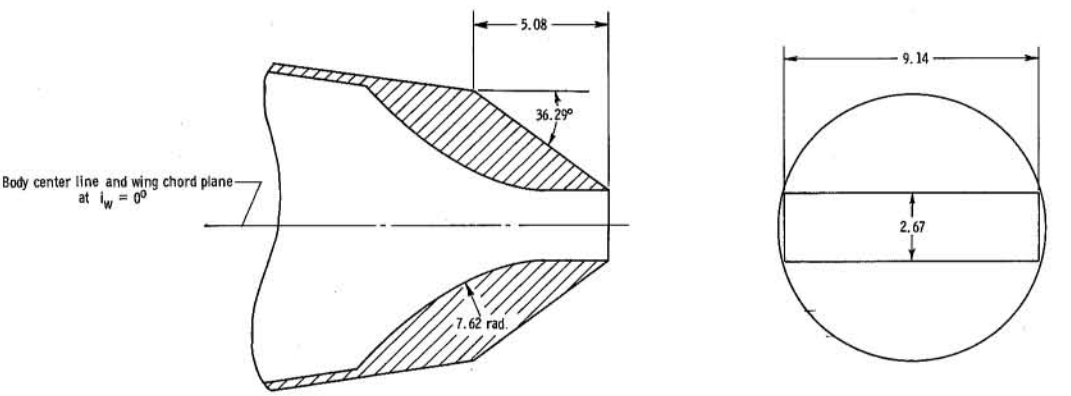

Section A-A for $\delta_d = 0°$, $A_e = 24.903\ cm^2$

δ_d, deg	a, cm	A_e, cm^2
5	2.149	24.968
10	1.976	24.774
15	1.788	25.774
20	1.588	25.097
25	1.407	24.258
30	1.140	25.290

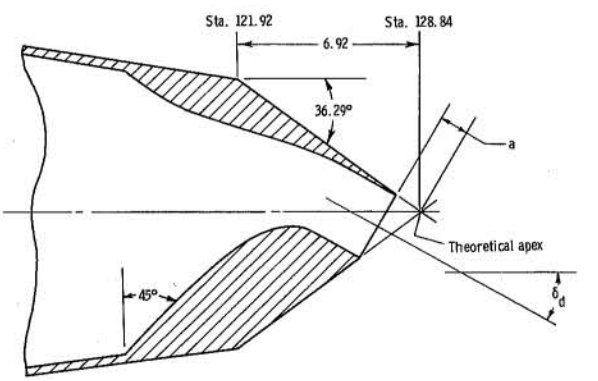

Typical section for deflected nozzles

Figure 5.- Nozzle geometry. All dimensions are in centimeters unless otherwise noted.

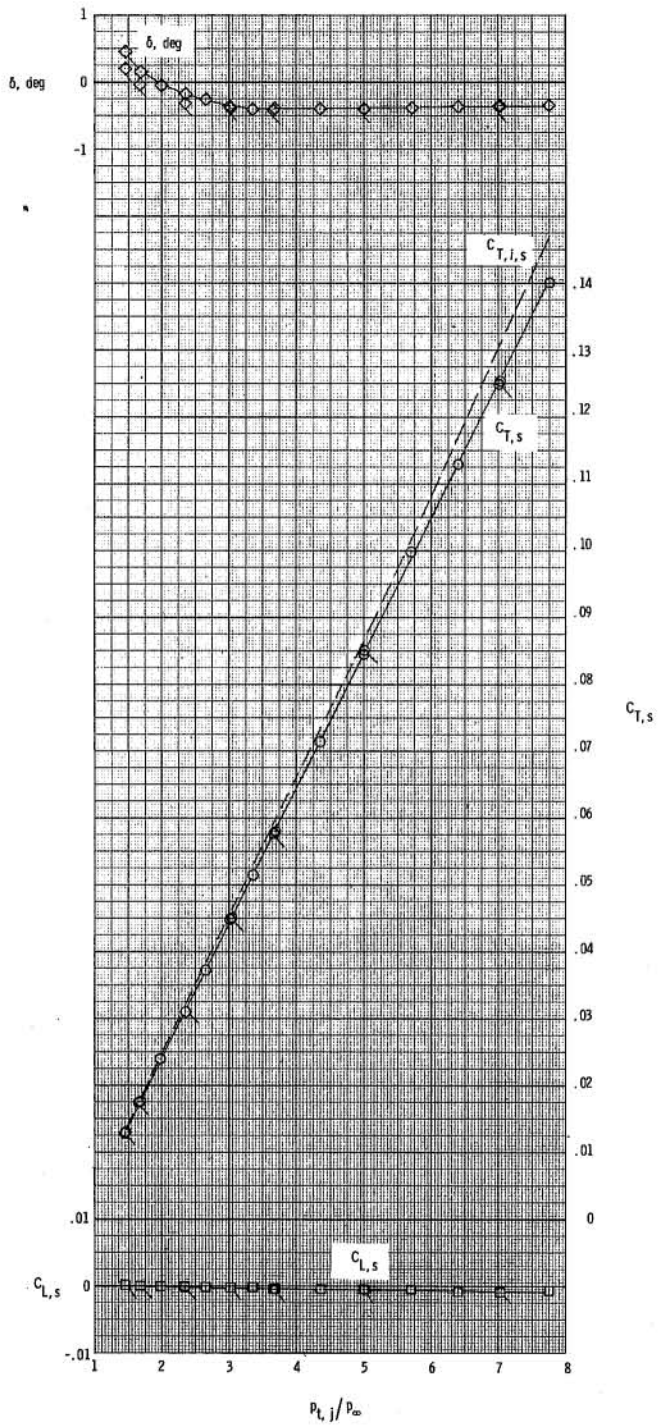

(a) $\delta_d = 0^o$.

Figure 6.- Nozzle static characteristics for various nominal exhaust-nozzle deflection angles. Symbols with ticks represent values at decreasing jet total-pressure ratio.

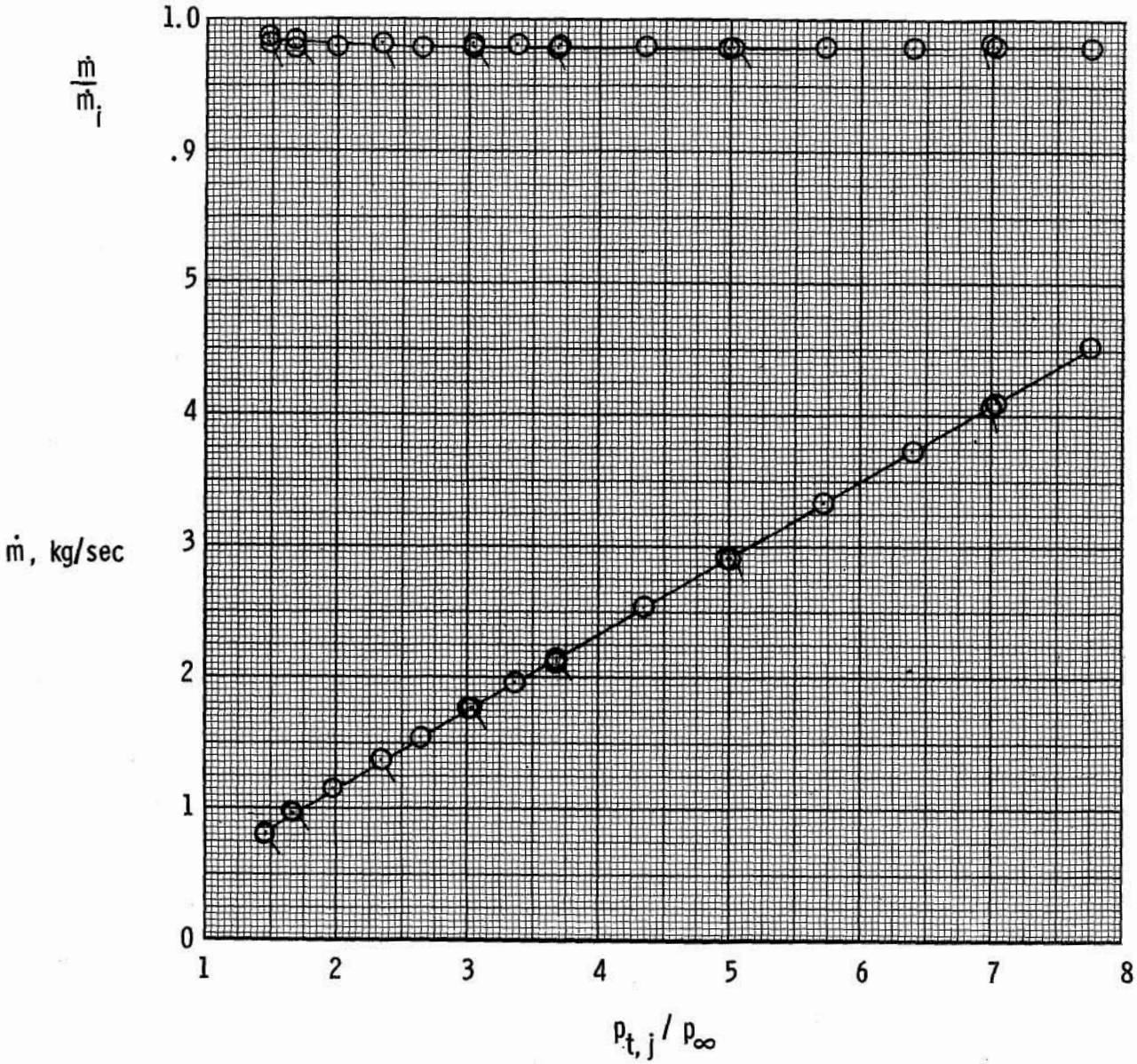

(a) $\delta_d = 0^o$. Concluded.

Figure 6.- Continued.

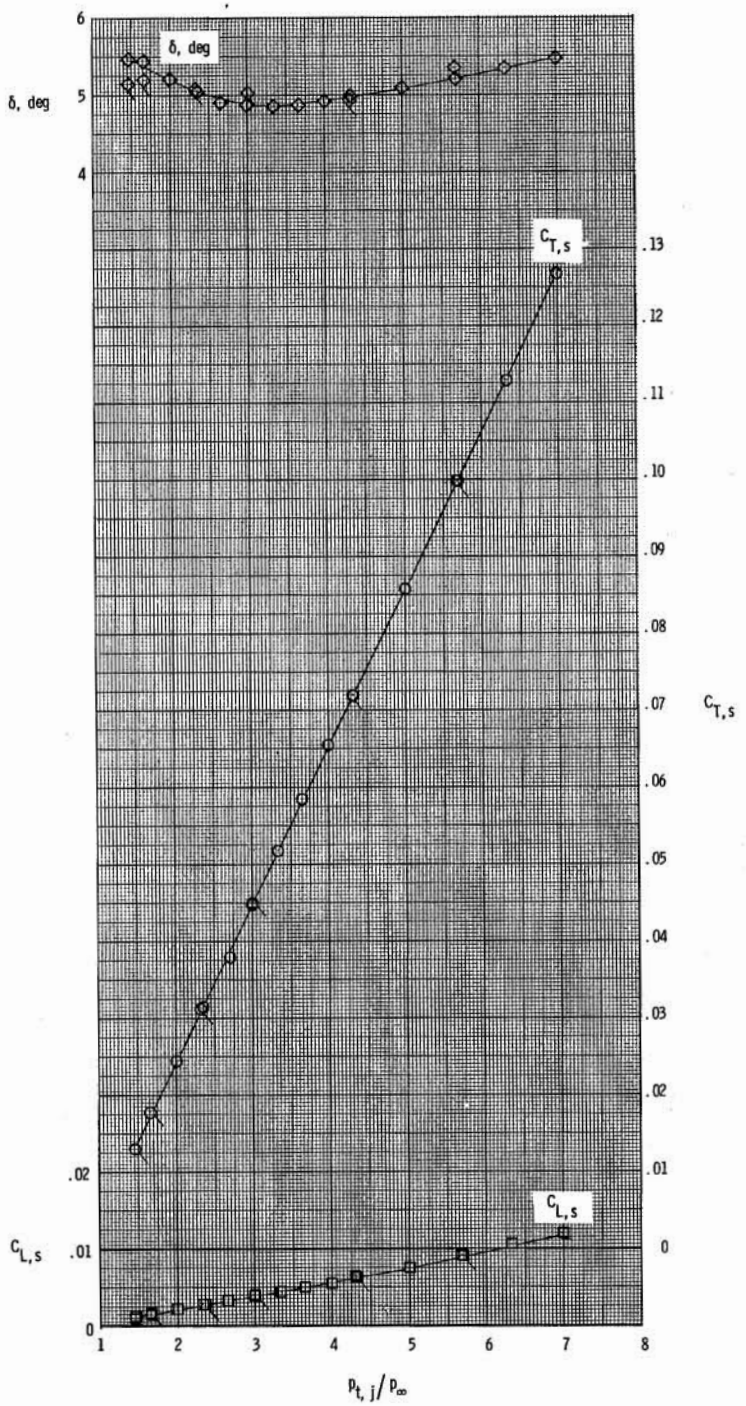

(b) $\delta_d = 5^o$.

Figure 6.- Continued.

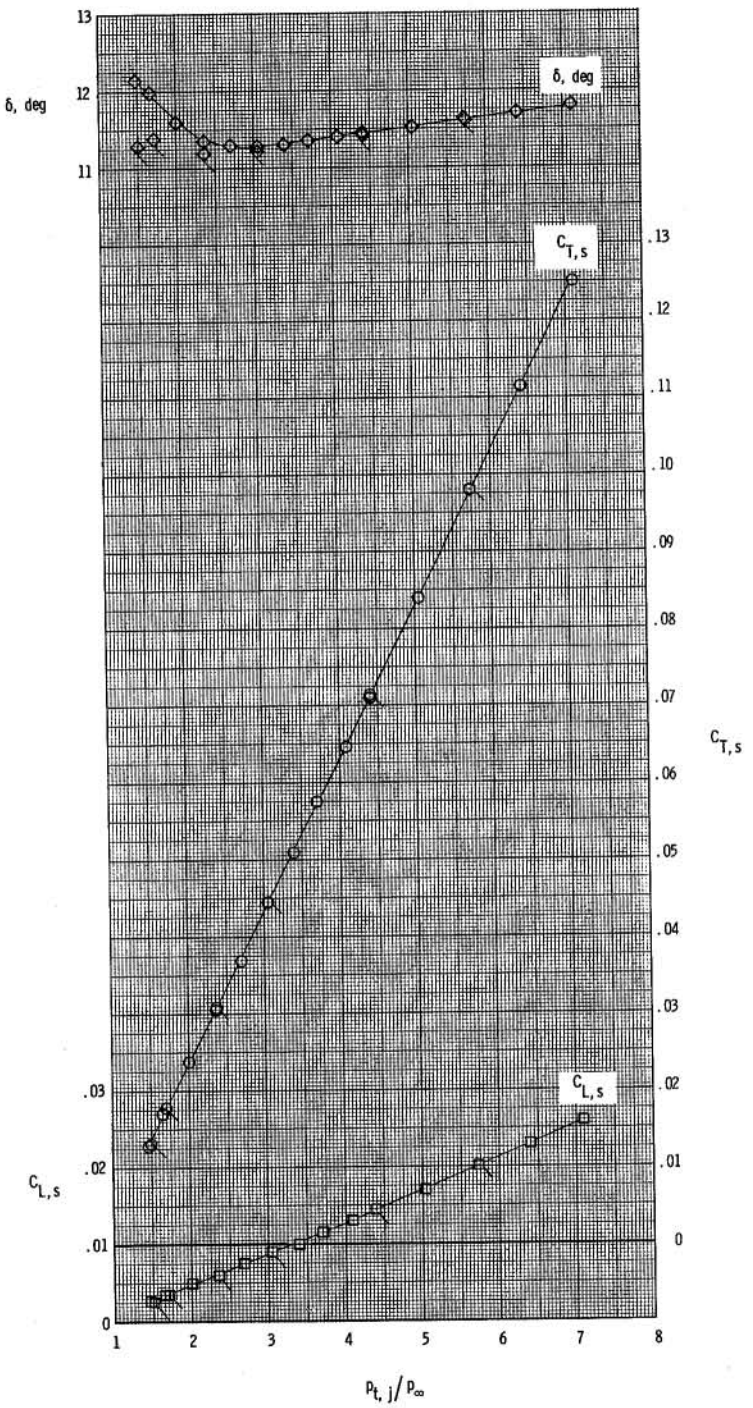

(c) $\delta_d = 10^o$.

Figure 6.- Continued.

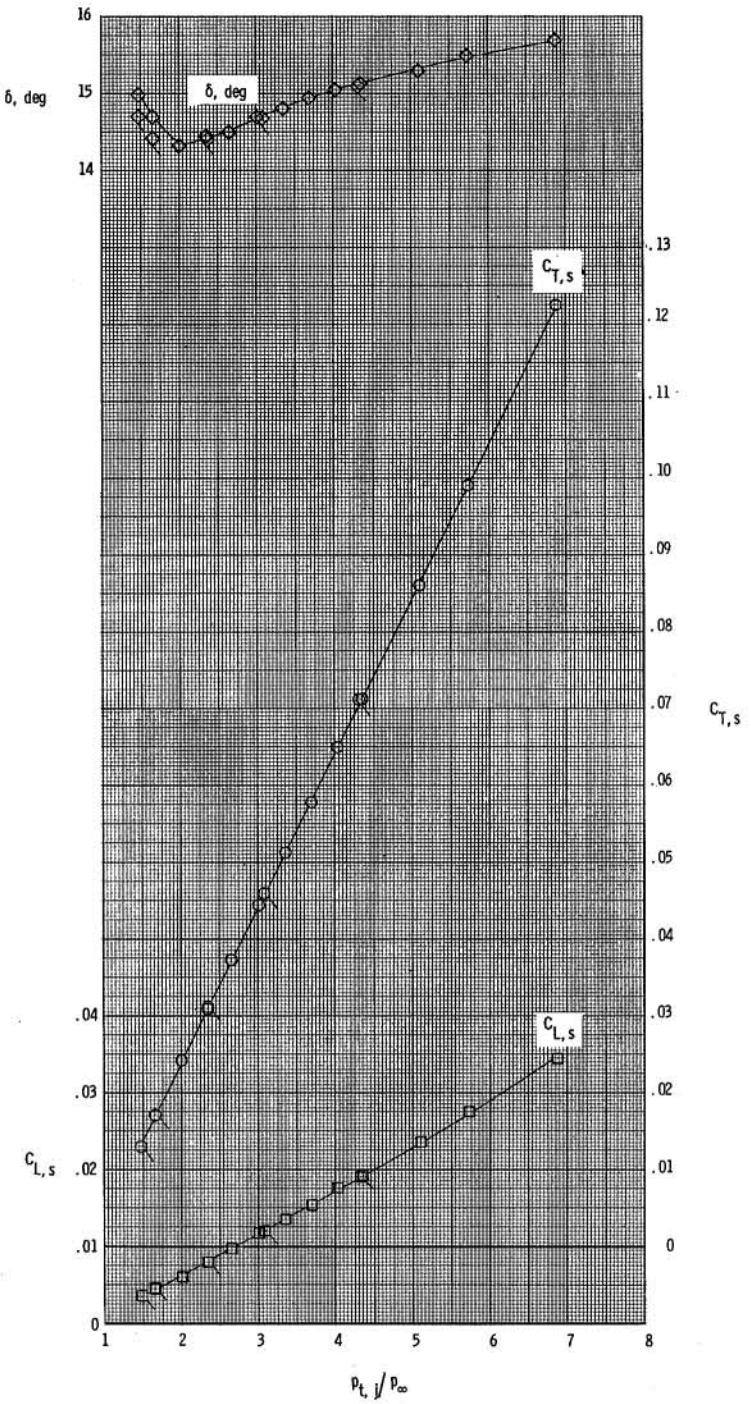

(d) $\delta_d = 15^o$.

Figure 6.- Continued.

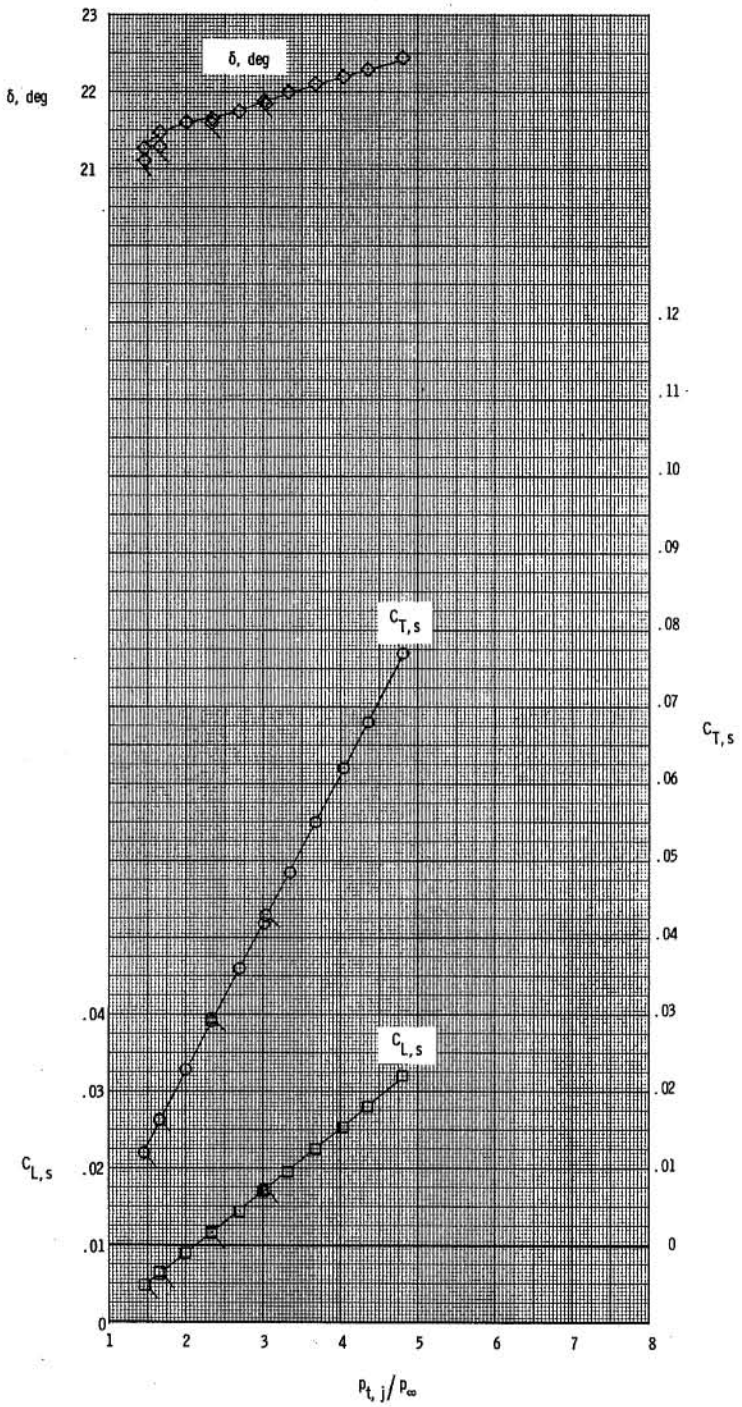

(e) $\delta_d = 20^o$.

Figure 6.- Continued.

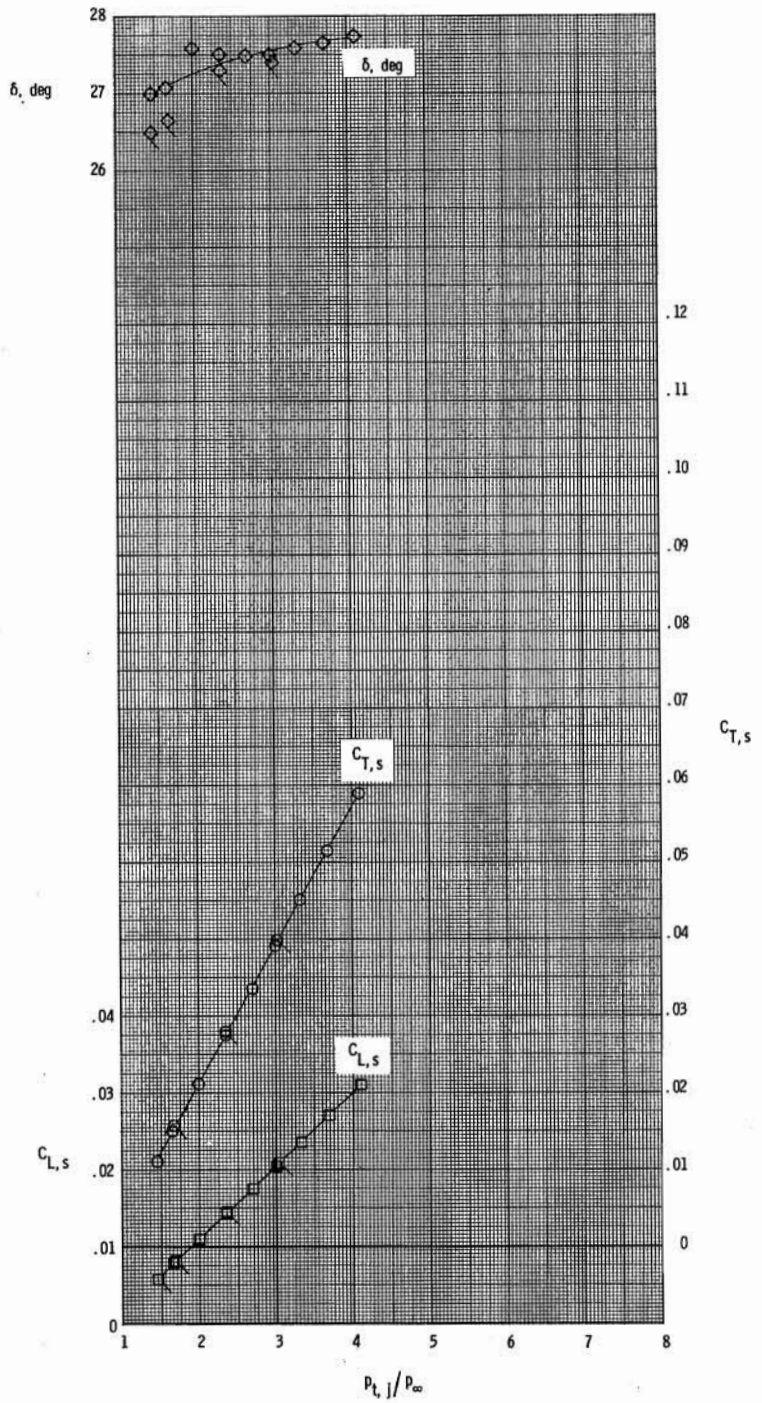

(f) $\delta_d = 25^o$.

Figure 6.- Continued.

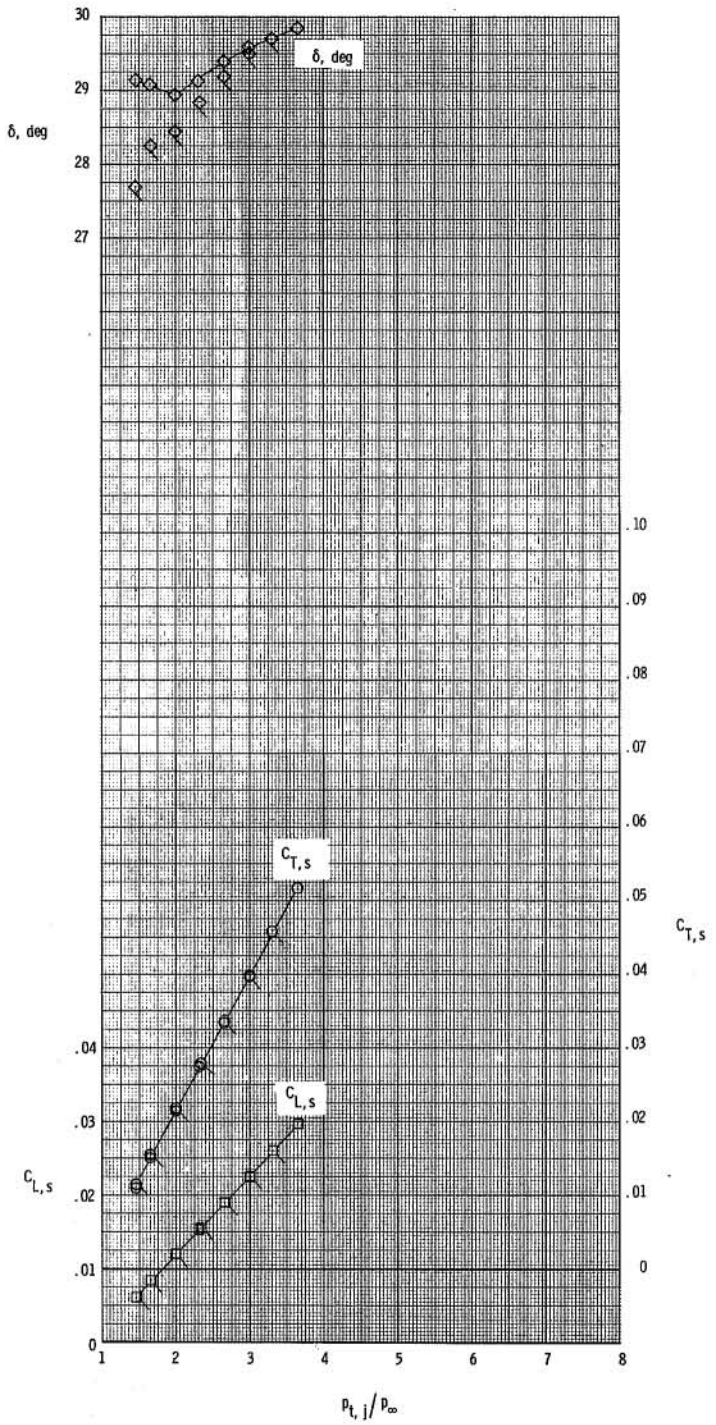

(g) $\delta_d = 30^o$.

Figure 6.- Concluded.

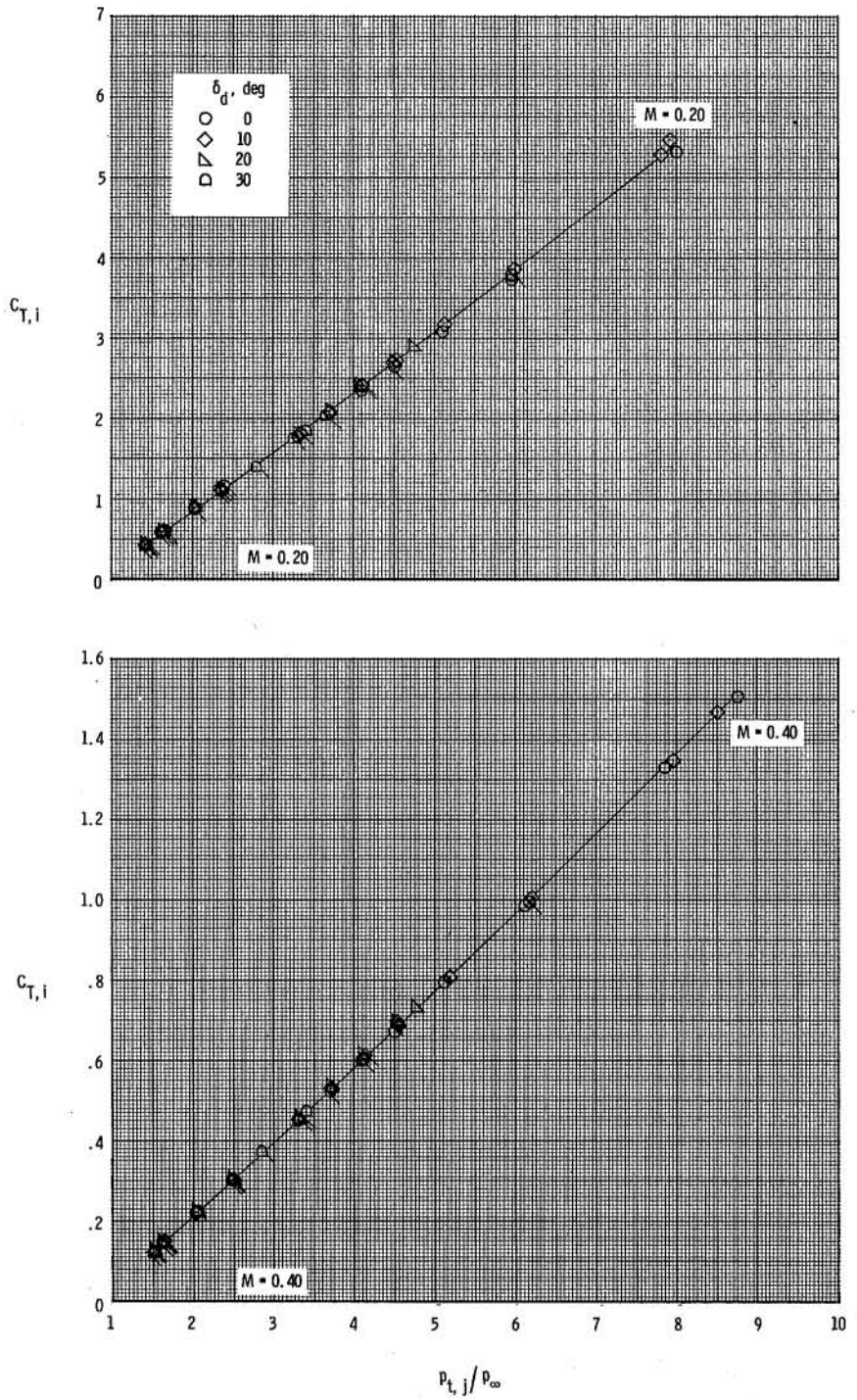

(a) M = 0.20 and 0.40.

Figure 7.- Variation of ideal gross thrust coefficient, mass-flow rate, and discharge coefficient with jet total-pressure ratio for selected exhaust-nozzle deflection angles. $i_w = -1.38^o$. Symbols with ticks represent values at decreasing jet total-pressure ratio.

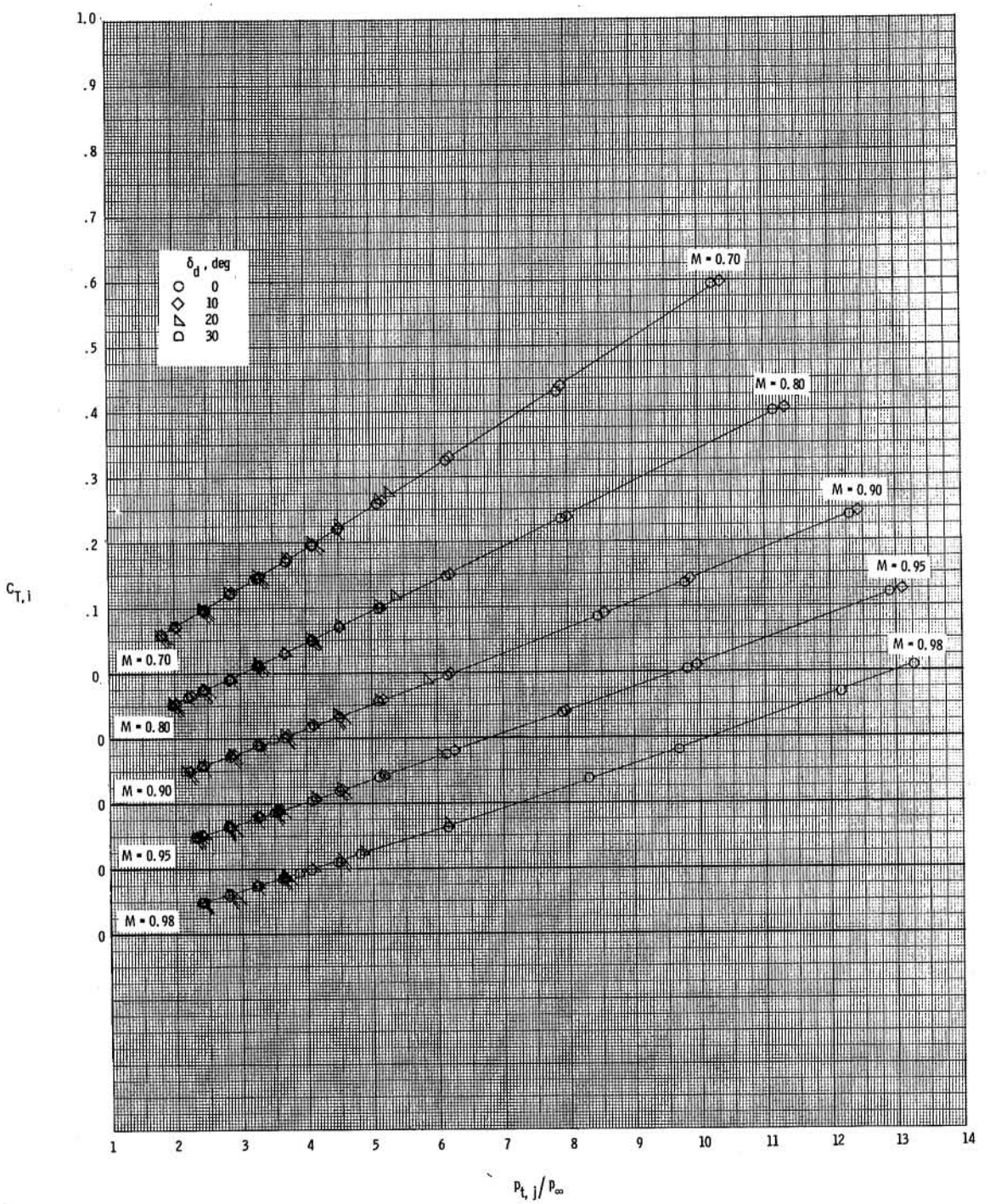

(b) M = 0.70 to 0.98.

Figure 7.- Continued.

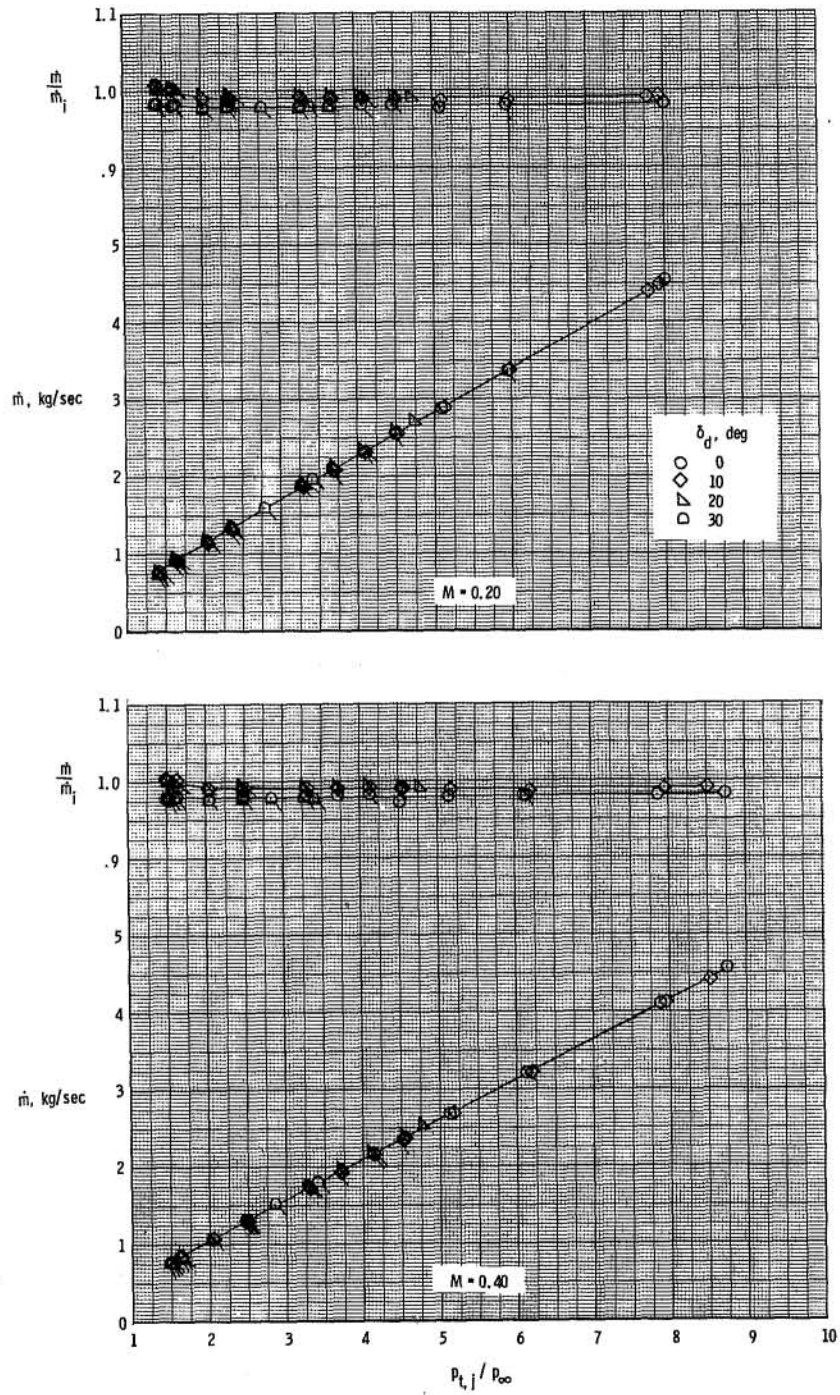

(c) M = 0.20 and 0.40.

Figure 7.- Continued.

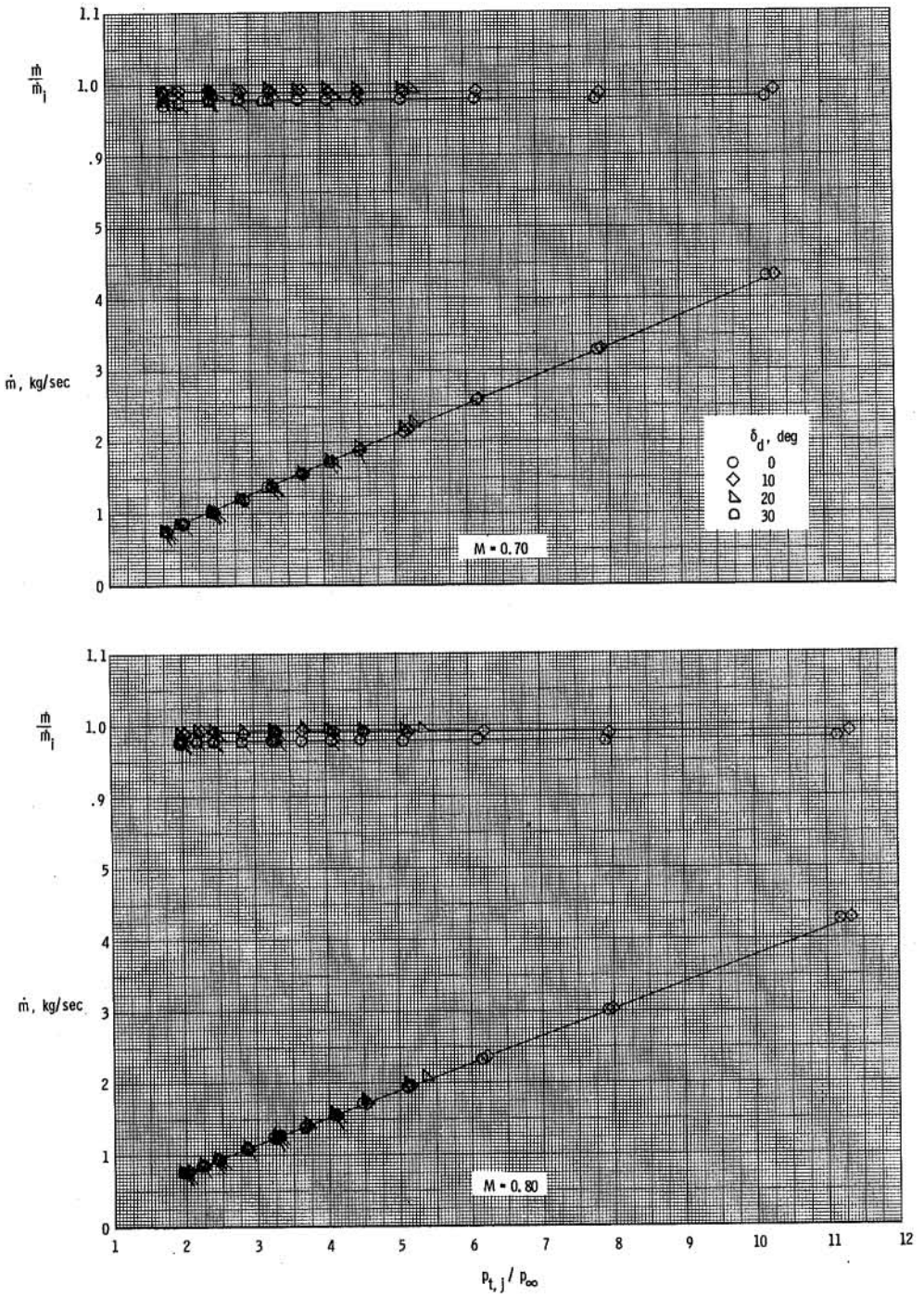

(d) M = 0.70 and 0.80.

Figure 7.- Continued.

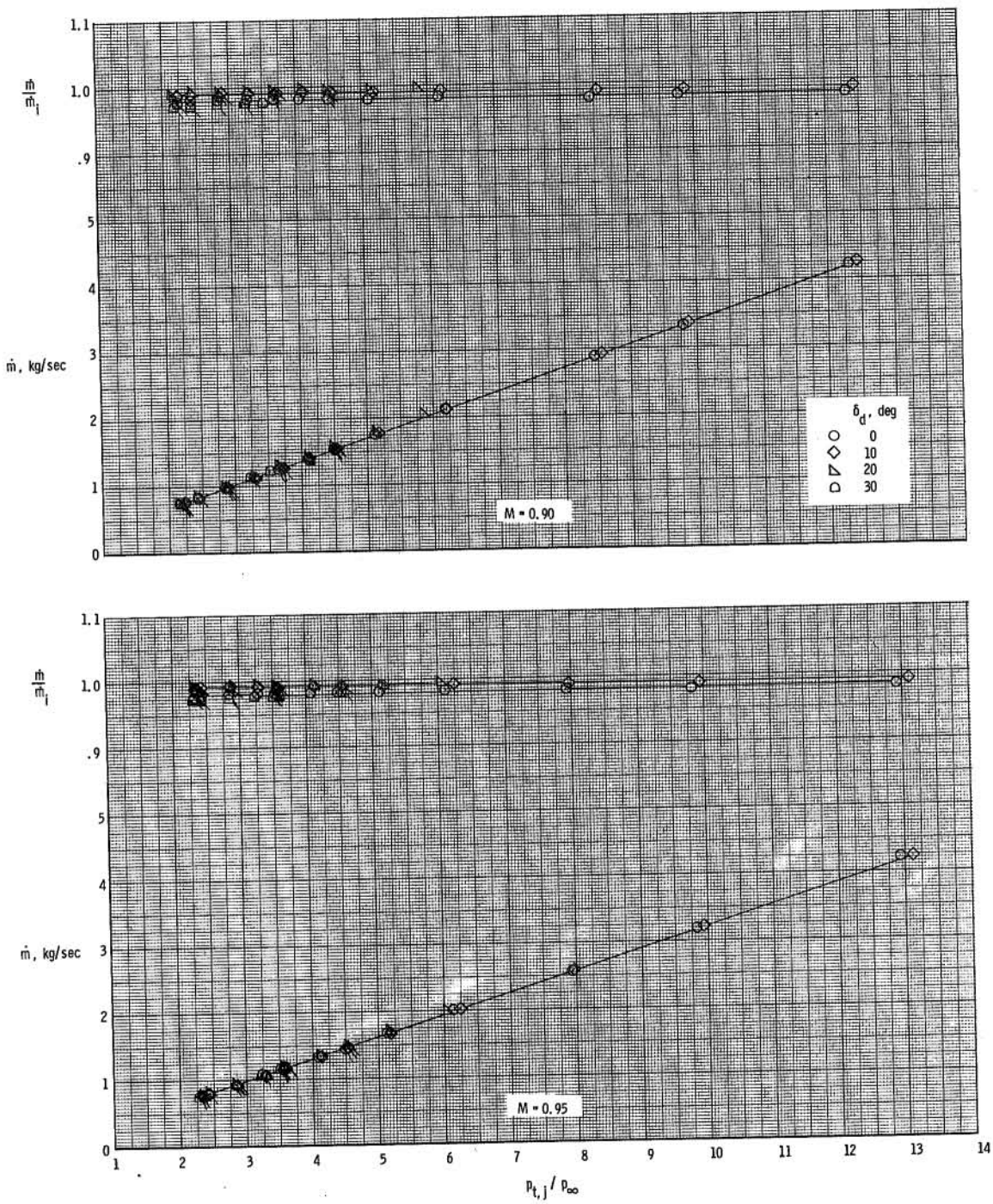

(e) M = 0.90 and 0.95.

Figure 7.- Continued.

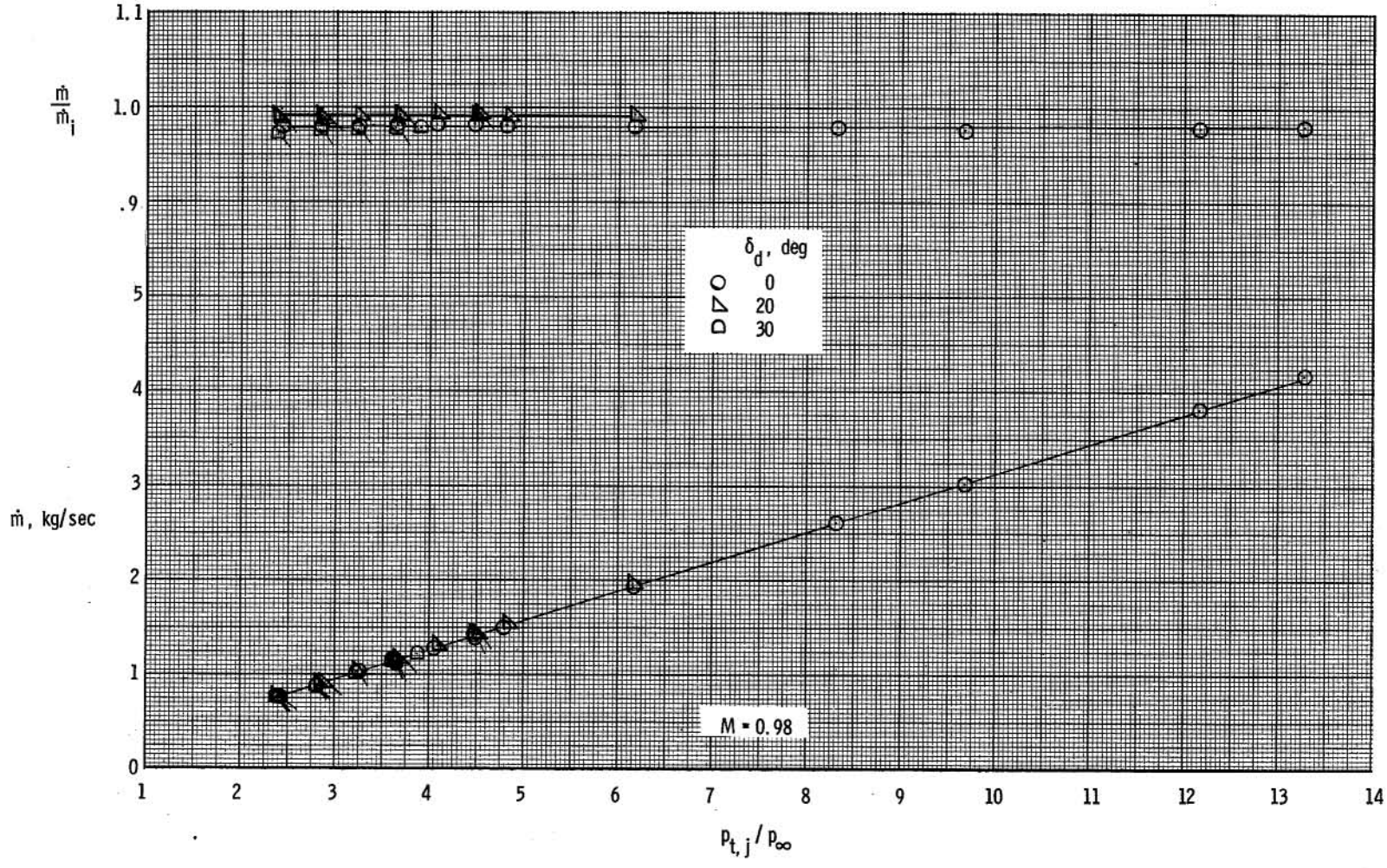

(f) M = 0.98.

Figure 7.- Concluded.

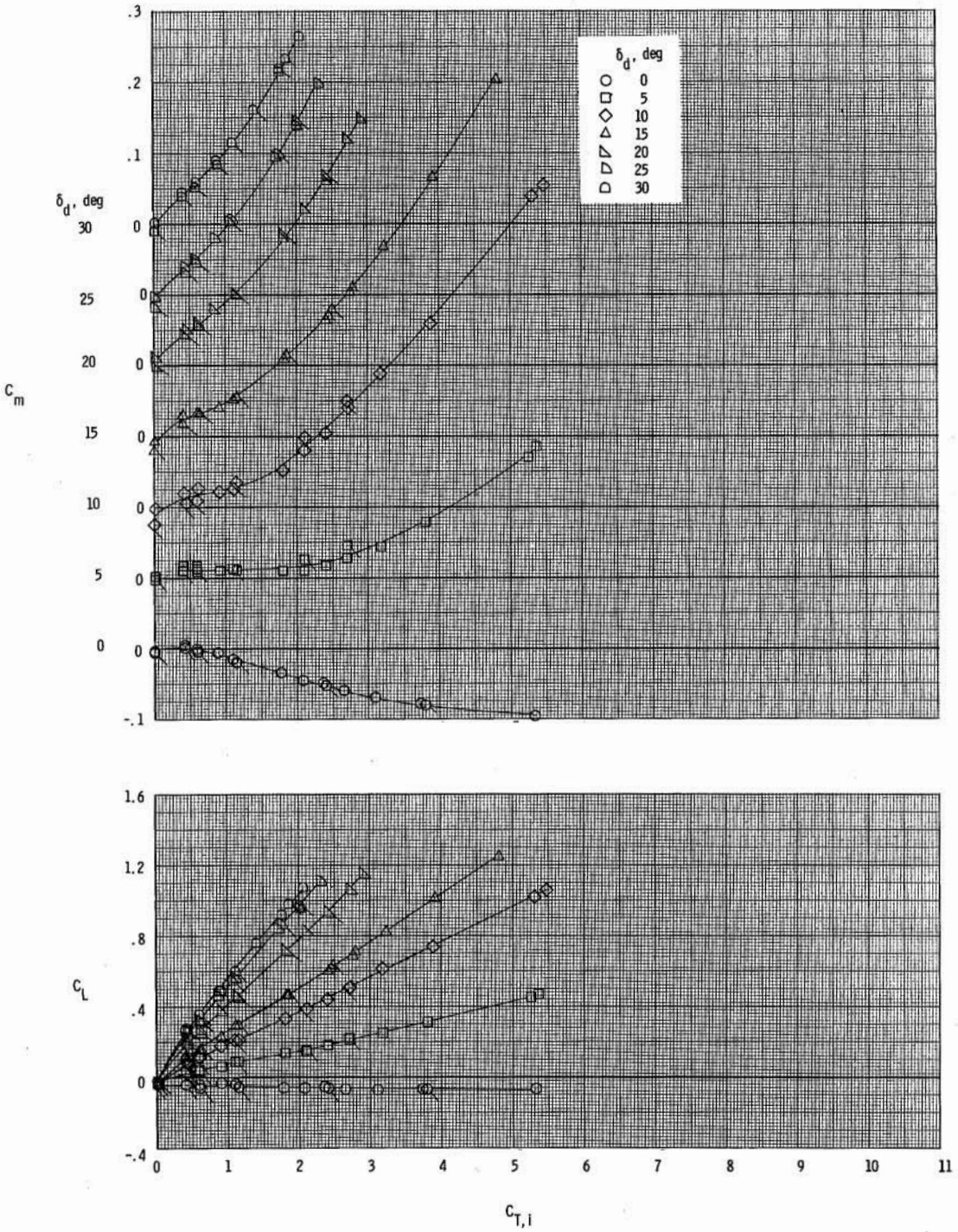

(a) M = 0.20.

Figure 8.- Variation of basic aerodynamic coefficients with ideal gross thrust coefficient for various exhaust-nozzle deflection angles. $i_w = -1.38^o$. Symbols with ticks represent values at decreasing jet total-pressure ratio.

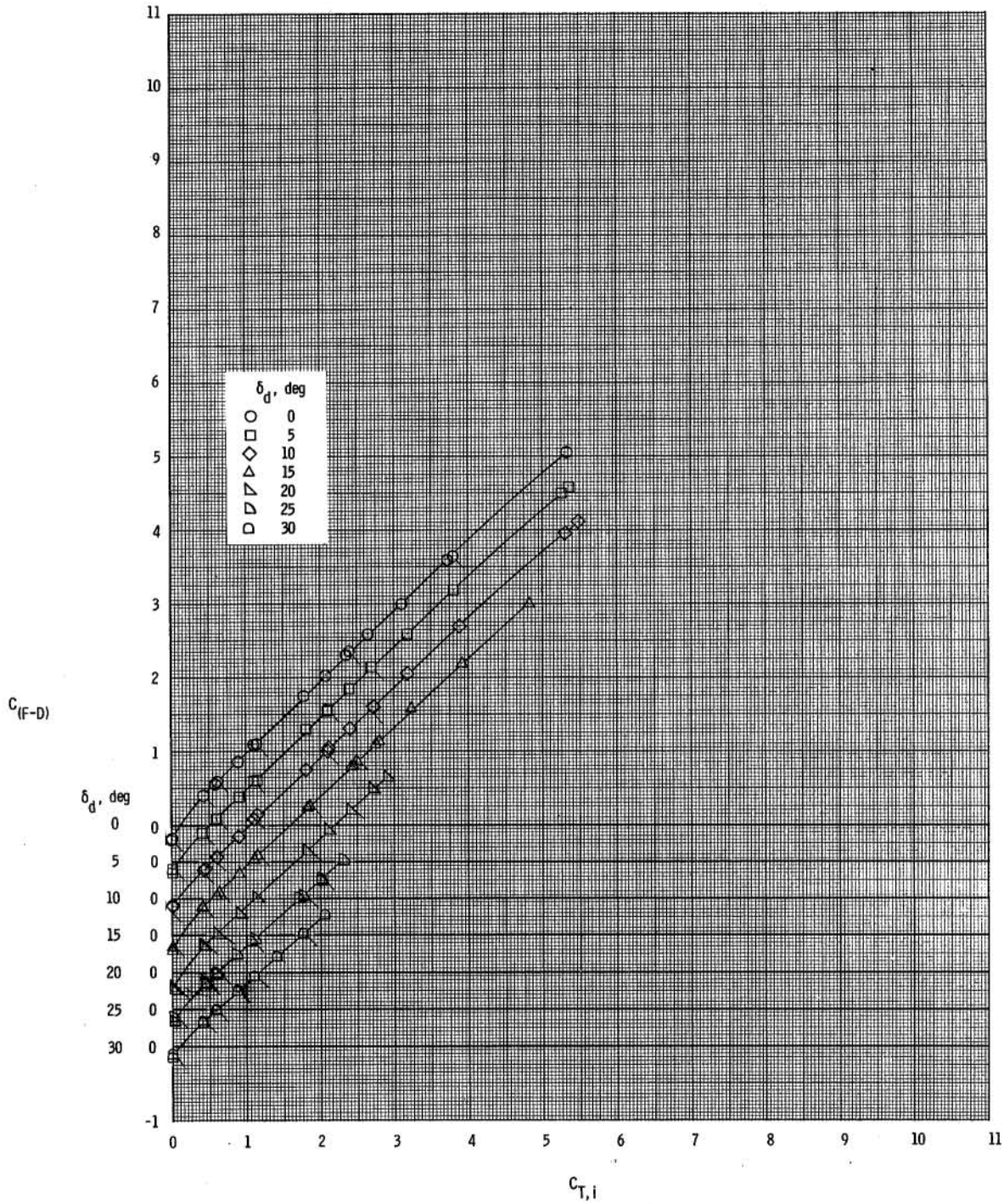

(a) M = 0.20. Concluded.

Figure 8.- Continued.

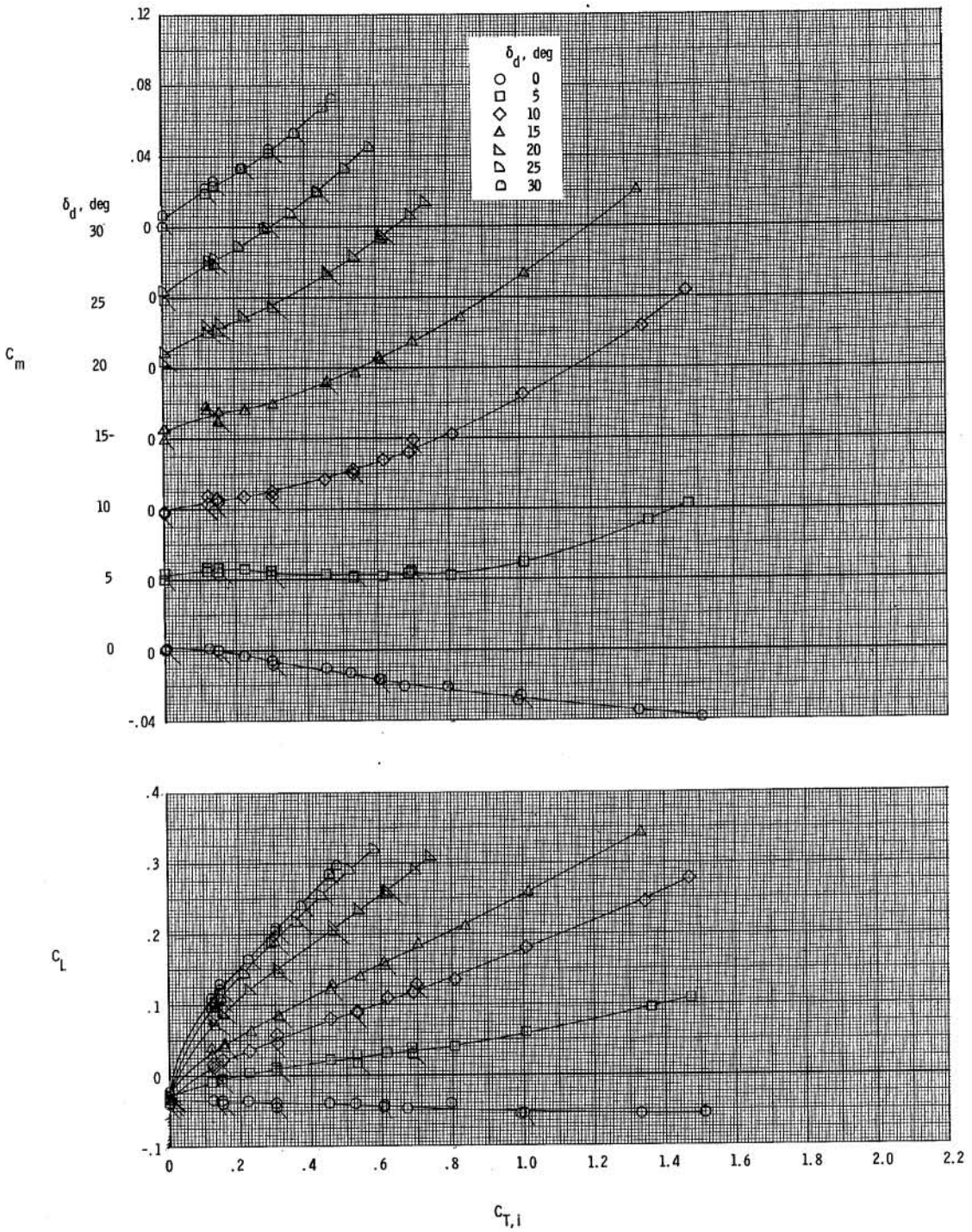

(b) M = 0.40.

Figure 8.- Continued.

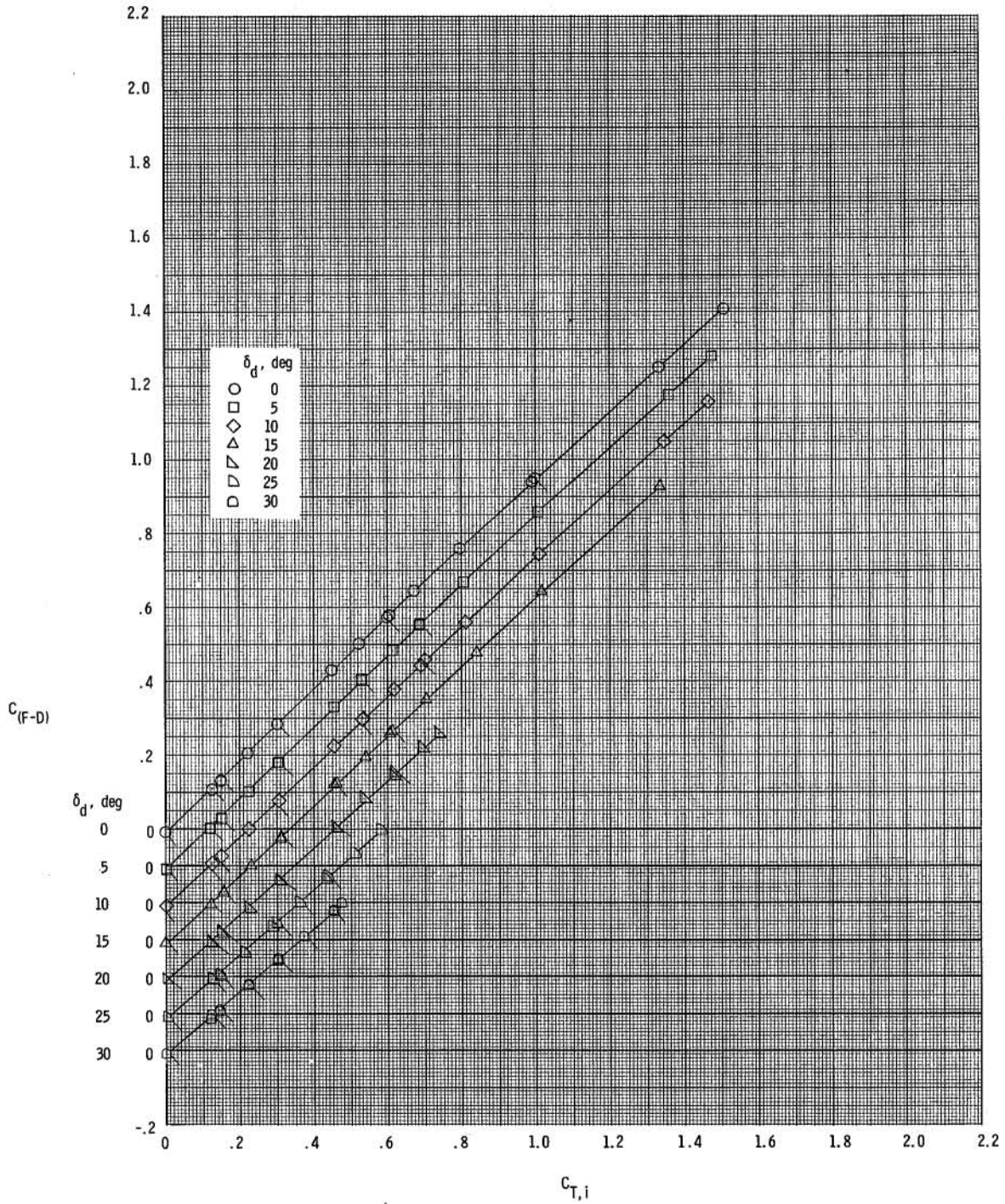

(b) M = 0.40. Concluded.

Figure 8.- Continued.

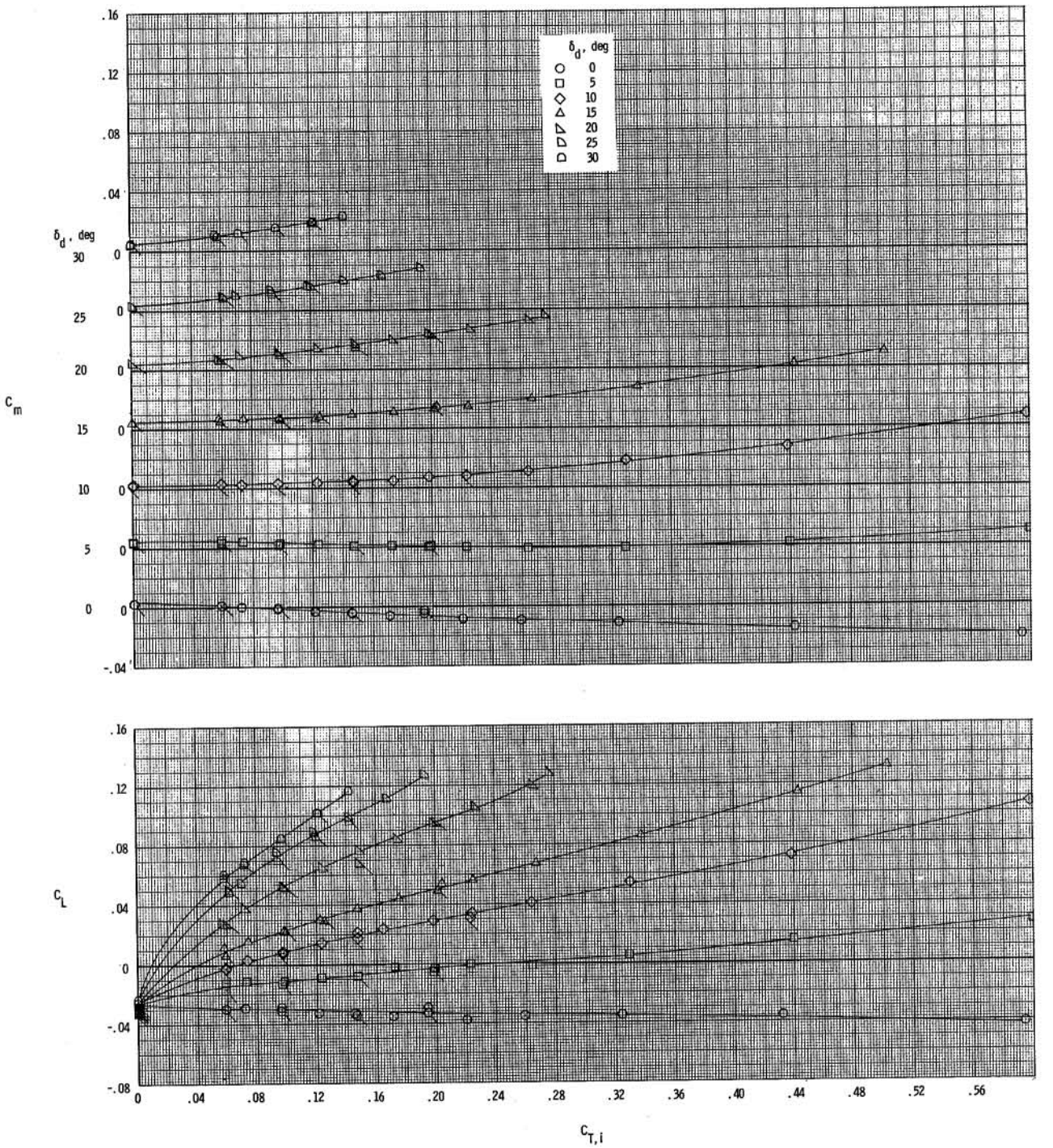

(c) M = 0.70.

Figure 8.- Continued.

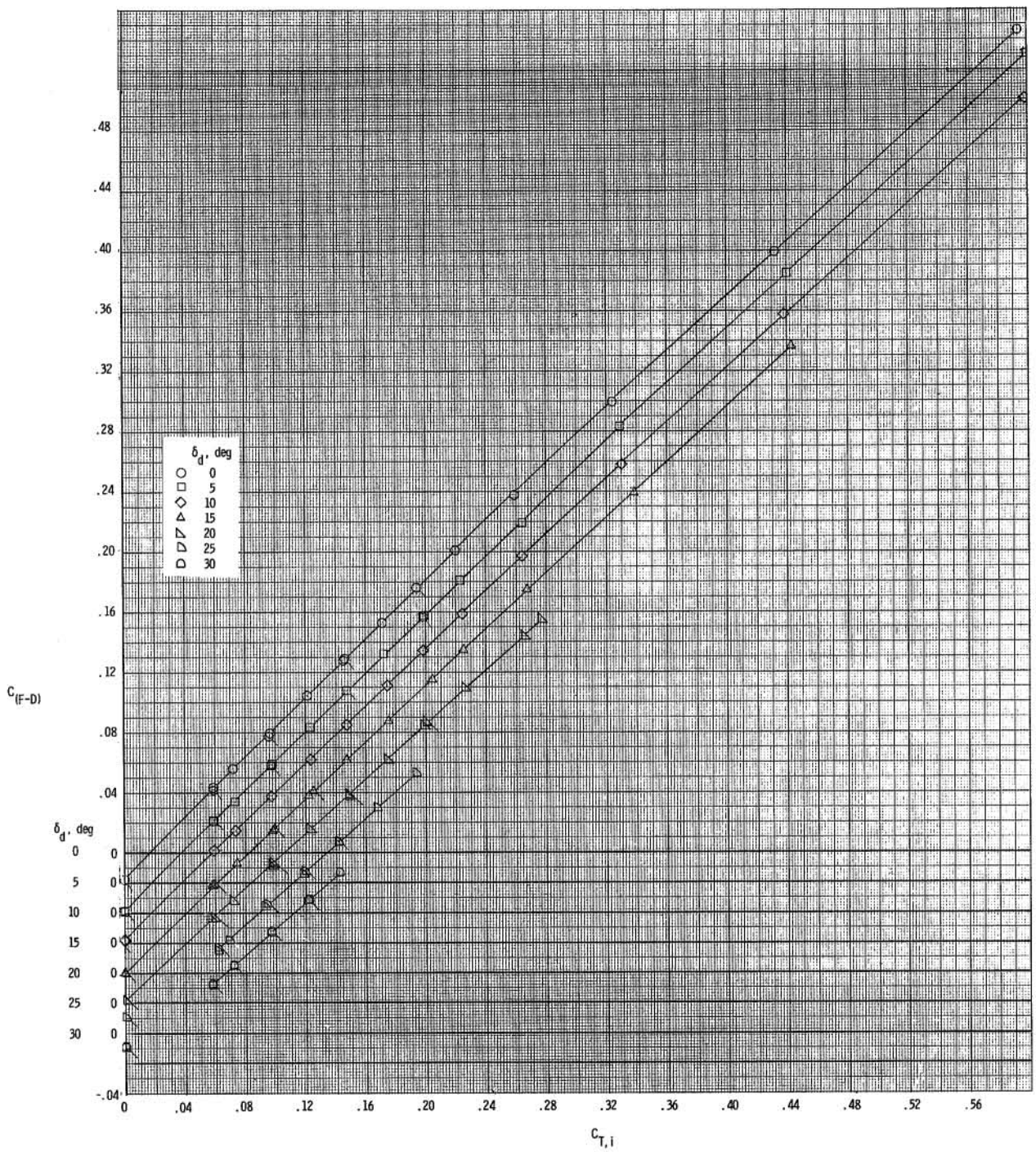

(c) M = 0.70. Concluded.

Figure 8.- Continued.

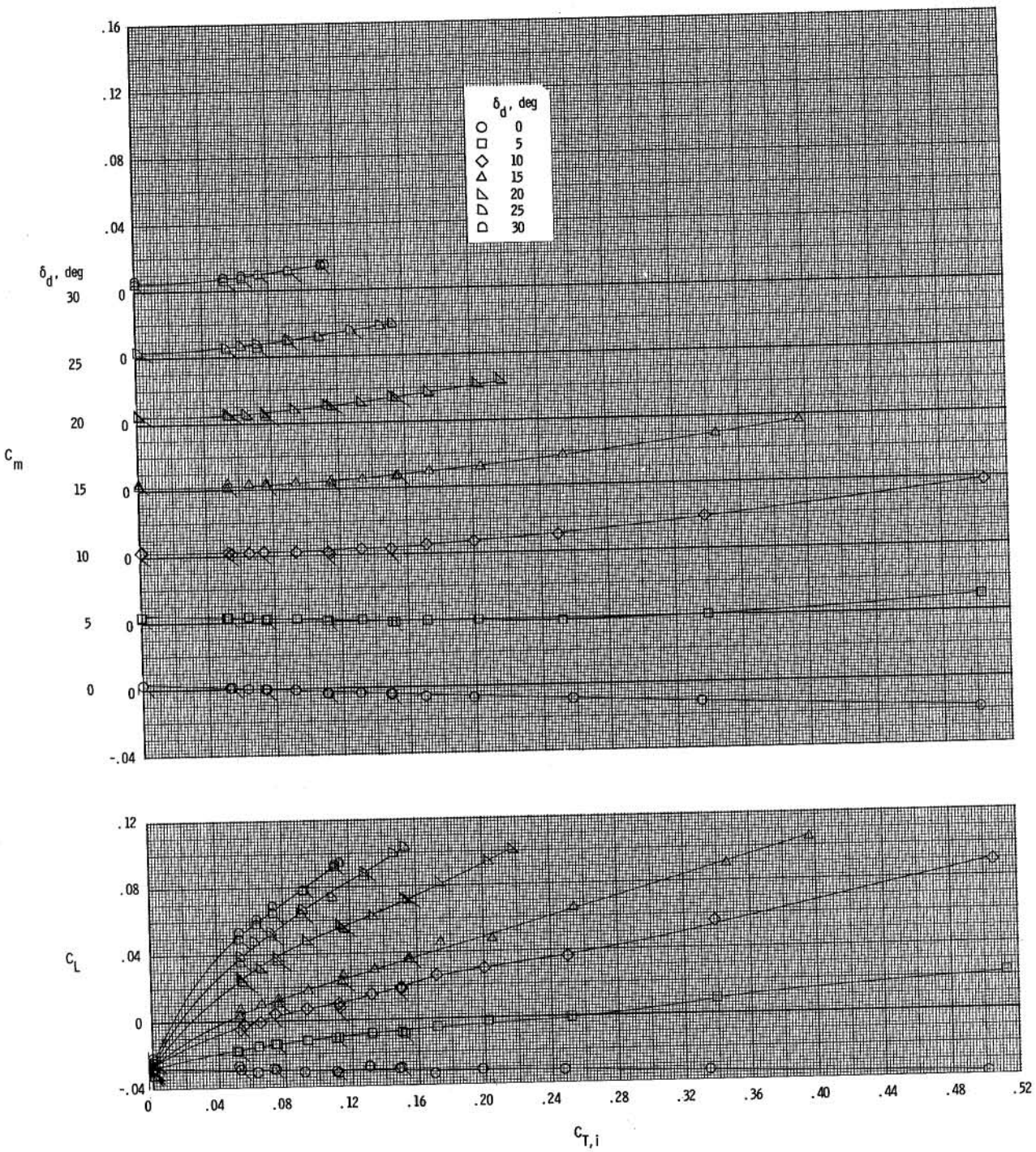

(d) M = 0.80.

Figure 8.- Continued.

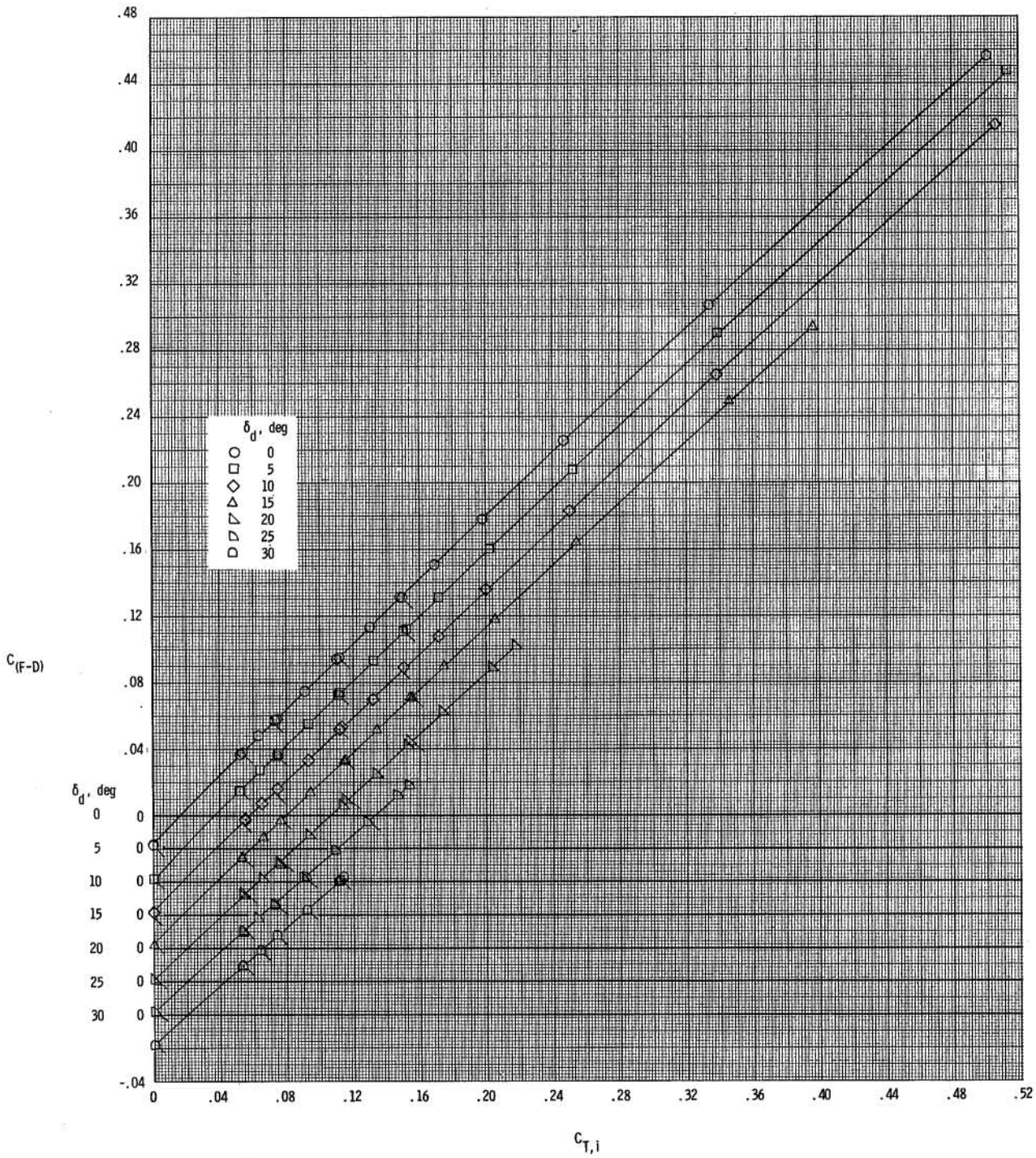

(d) M = 0.80. Concluded.

Figure 8.- Continued.

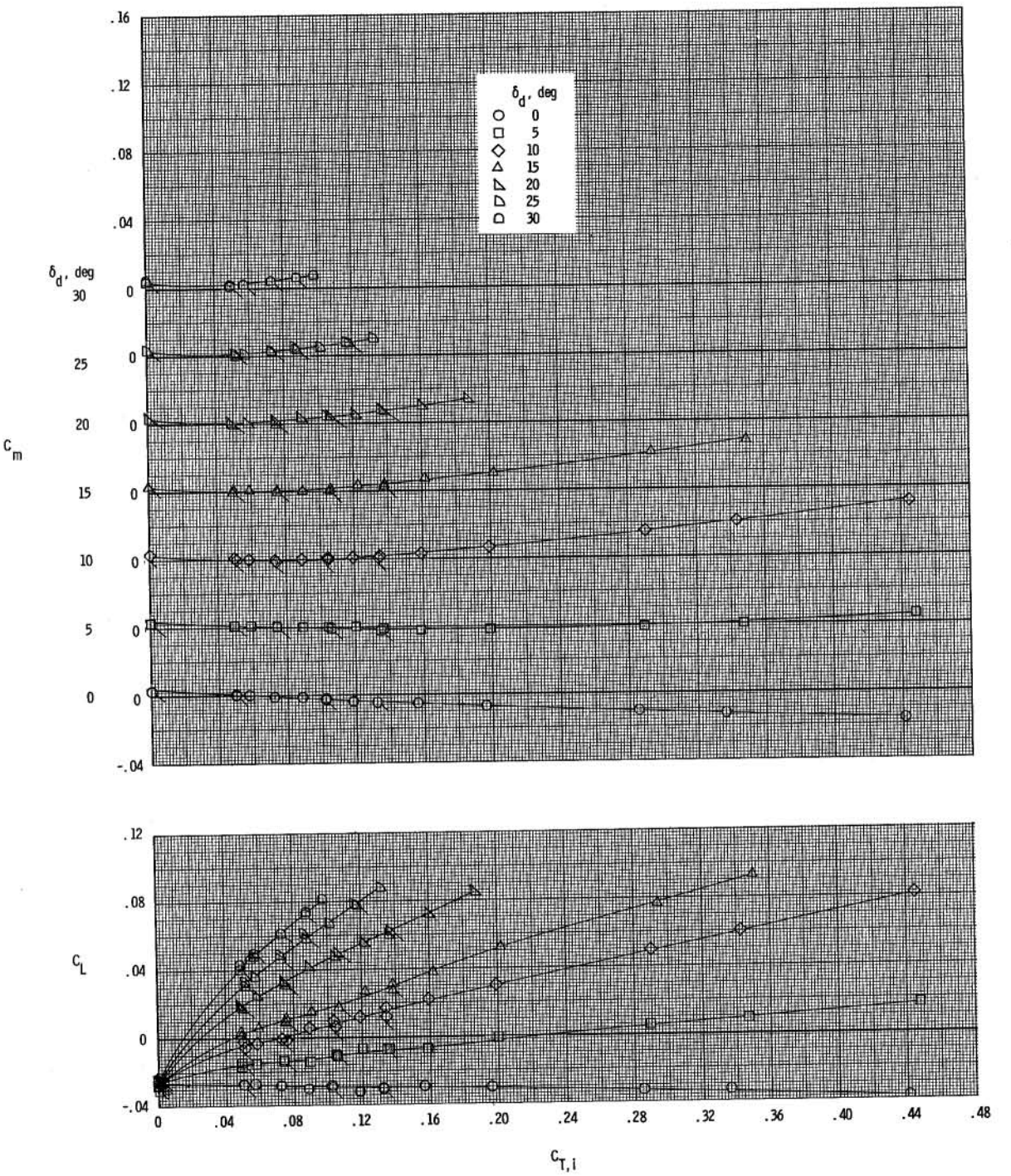

(e) M = 0.90.

Figure 8.- Continued.

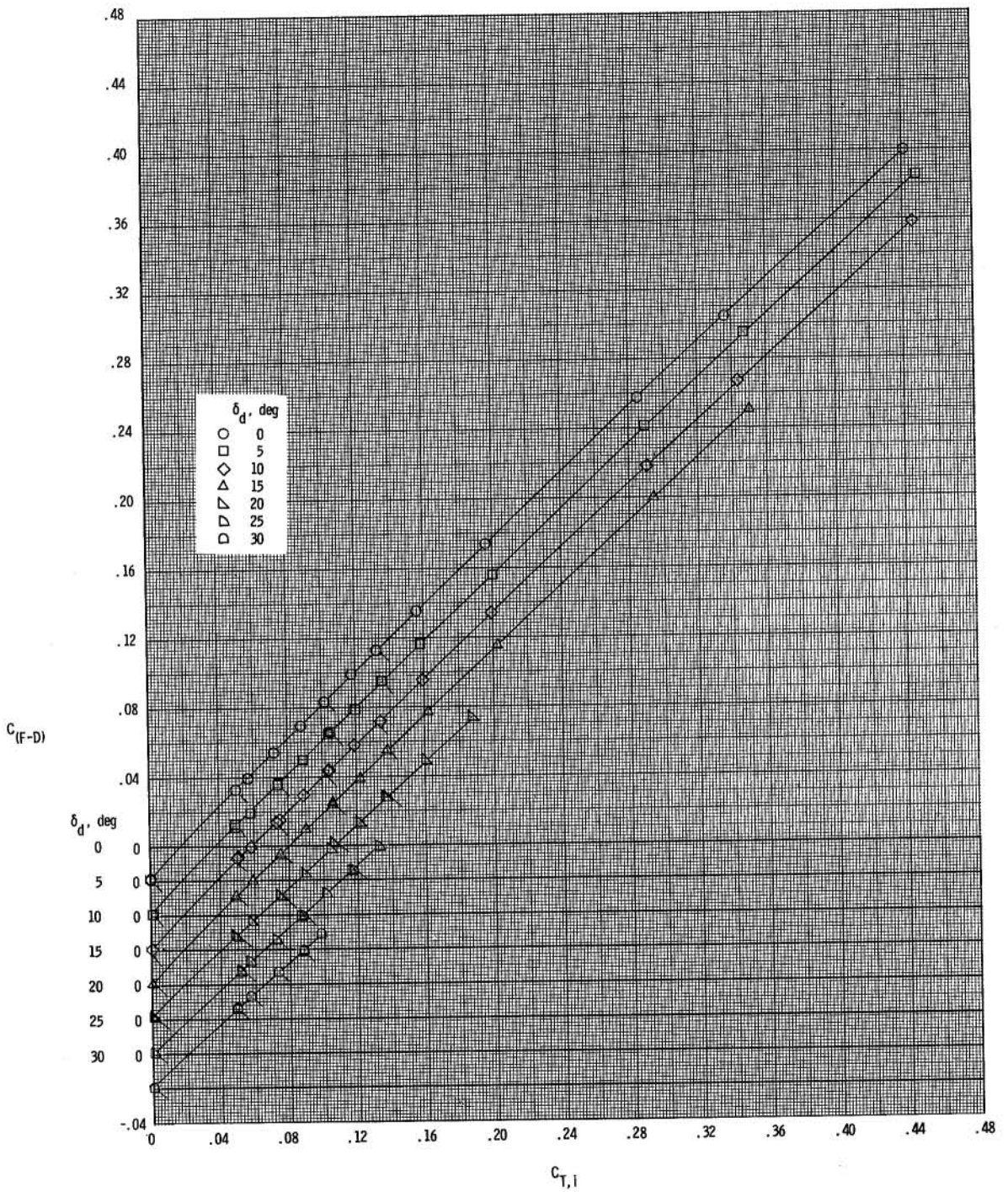

(e) M = 0.90. Concluded.

Figure 8.- Continued.

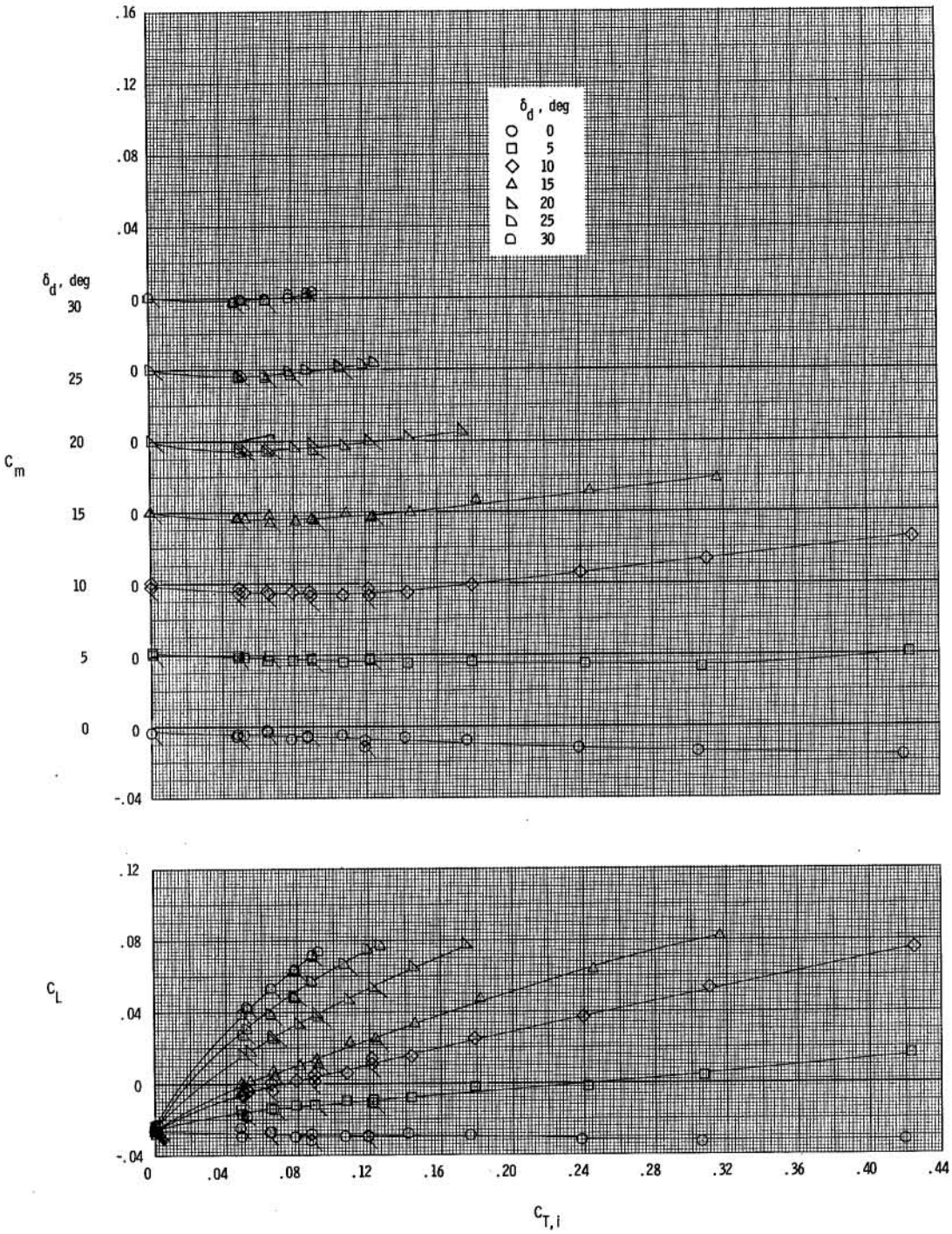

(f) M = 0.95.

Figure 8.- Continued.

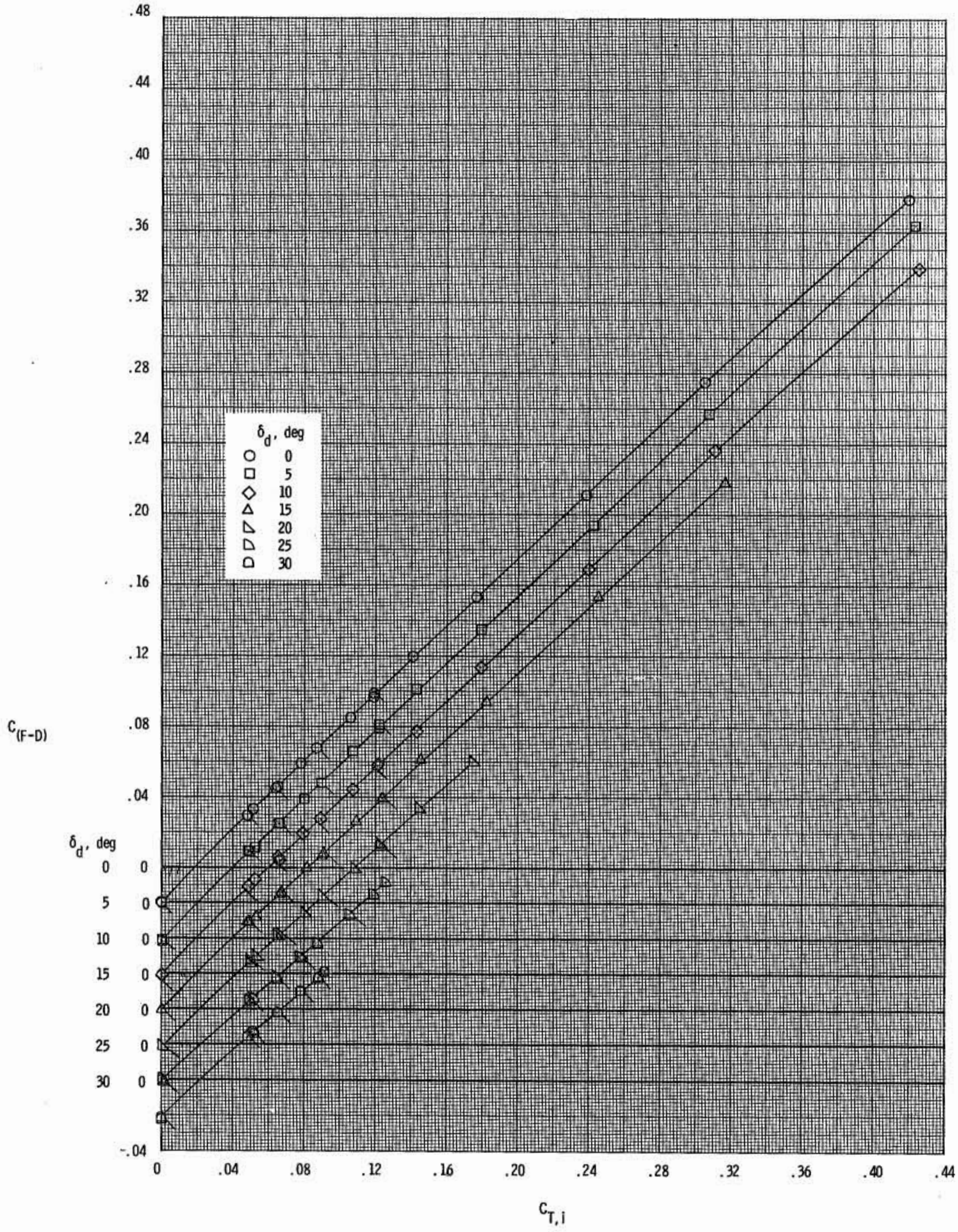

(f) M = 0.95. Concluded.

Figure 8.- Continued.

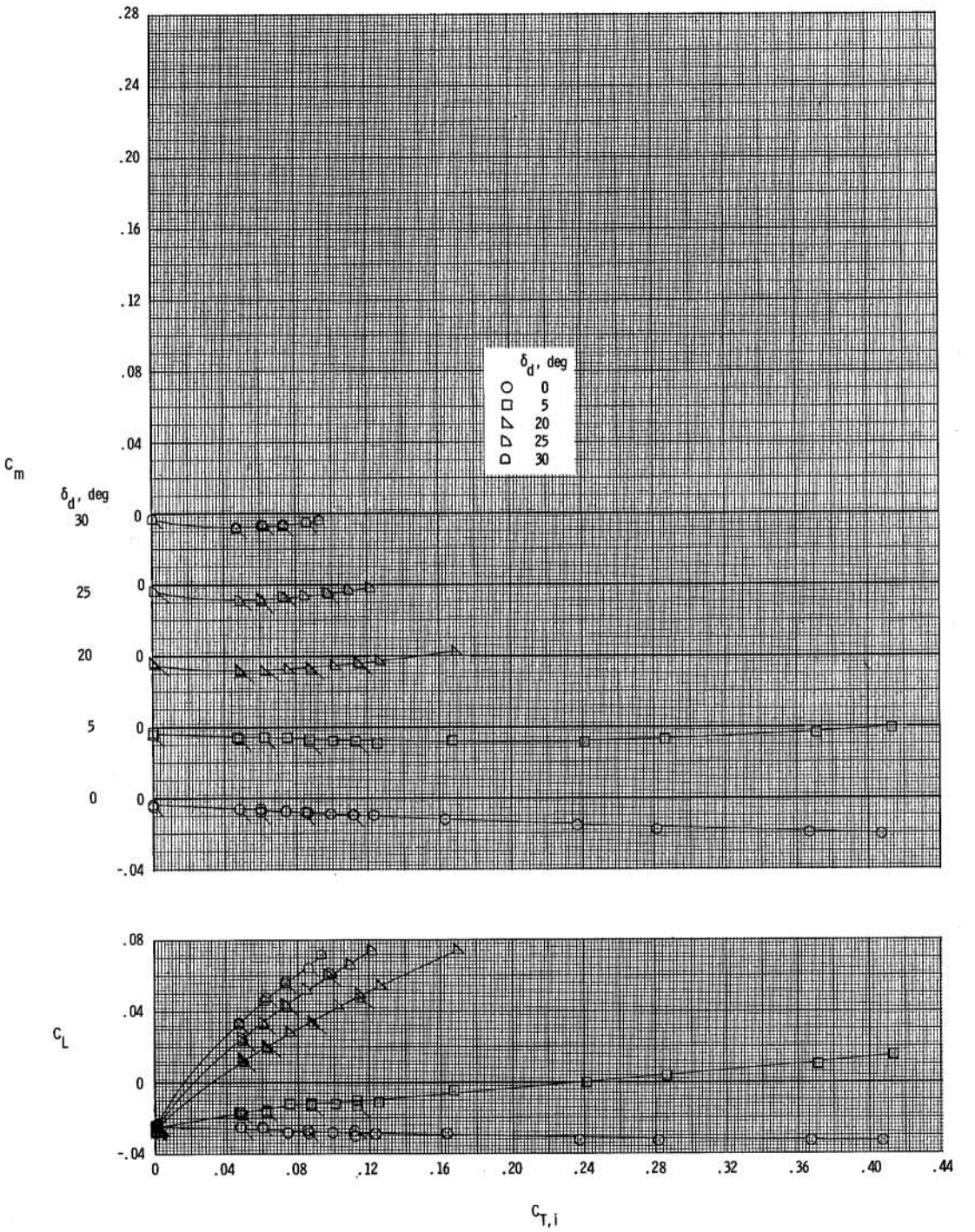

(g) M = 0.98.

Figure 8.- Continued.

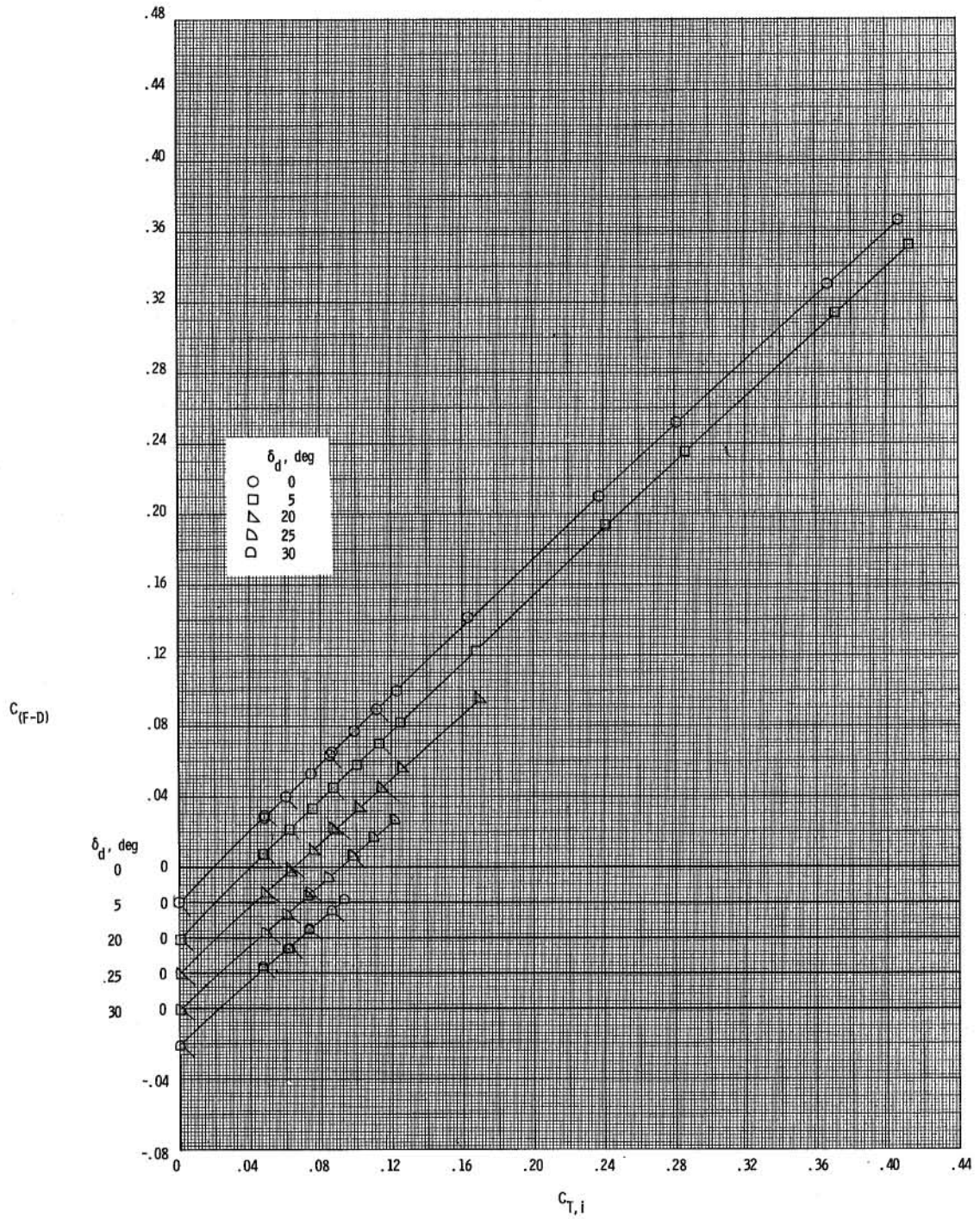

(g) M = 0.98. Concluded.

Figure 8.- Concluded.

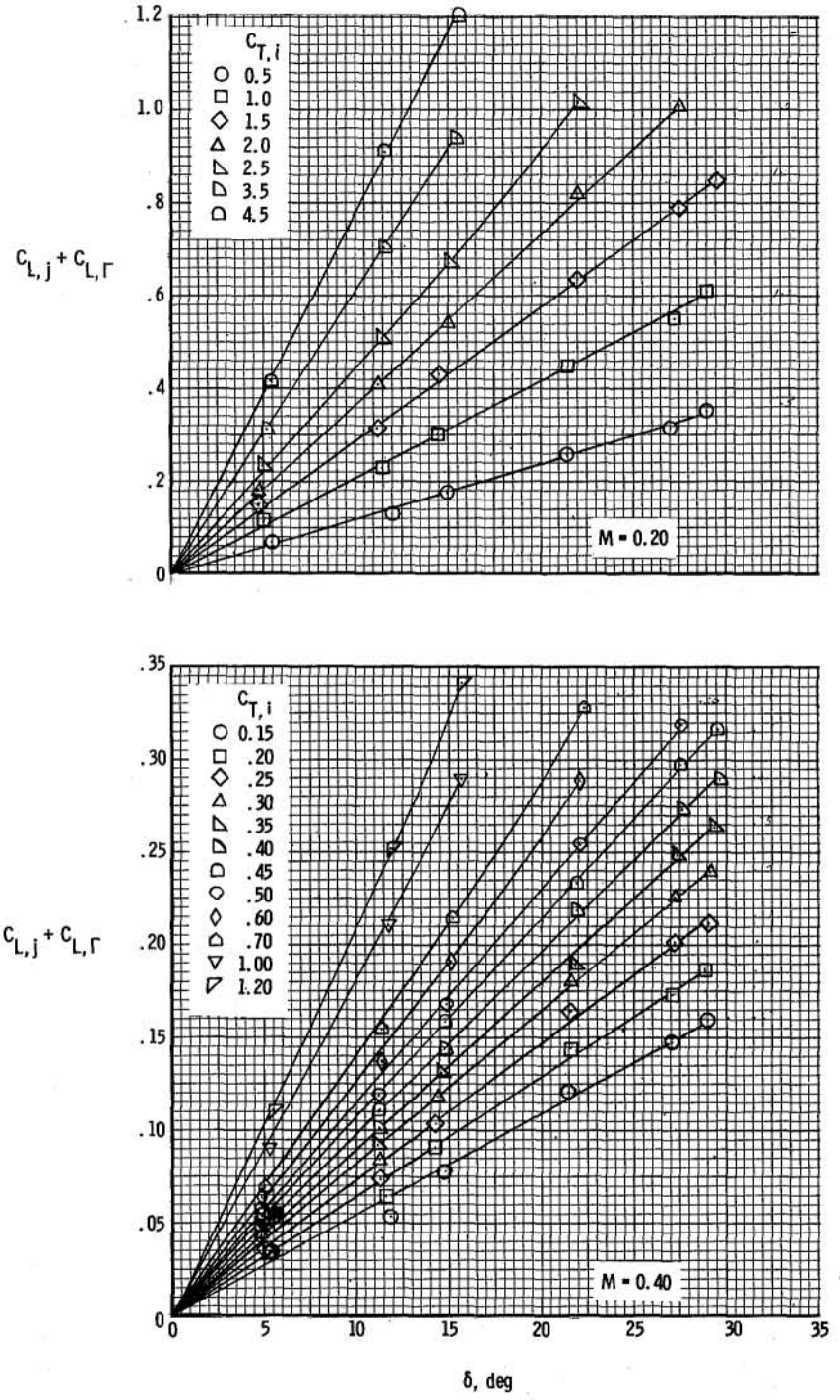

(a) M = 0.20 and 0.40.

Figure 9.- Variation of jet lift plus jet-circulation lift with measured nozzle deflection angle. $i_w = -1.38$. (Symbols represent interpolated values.)

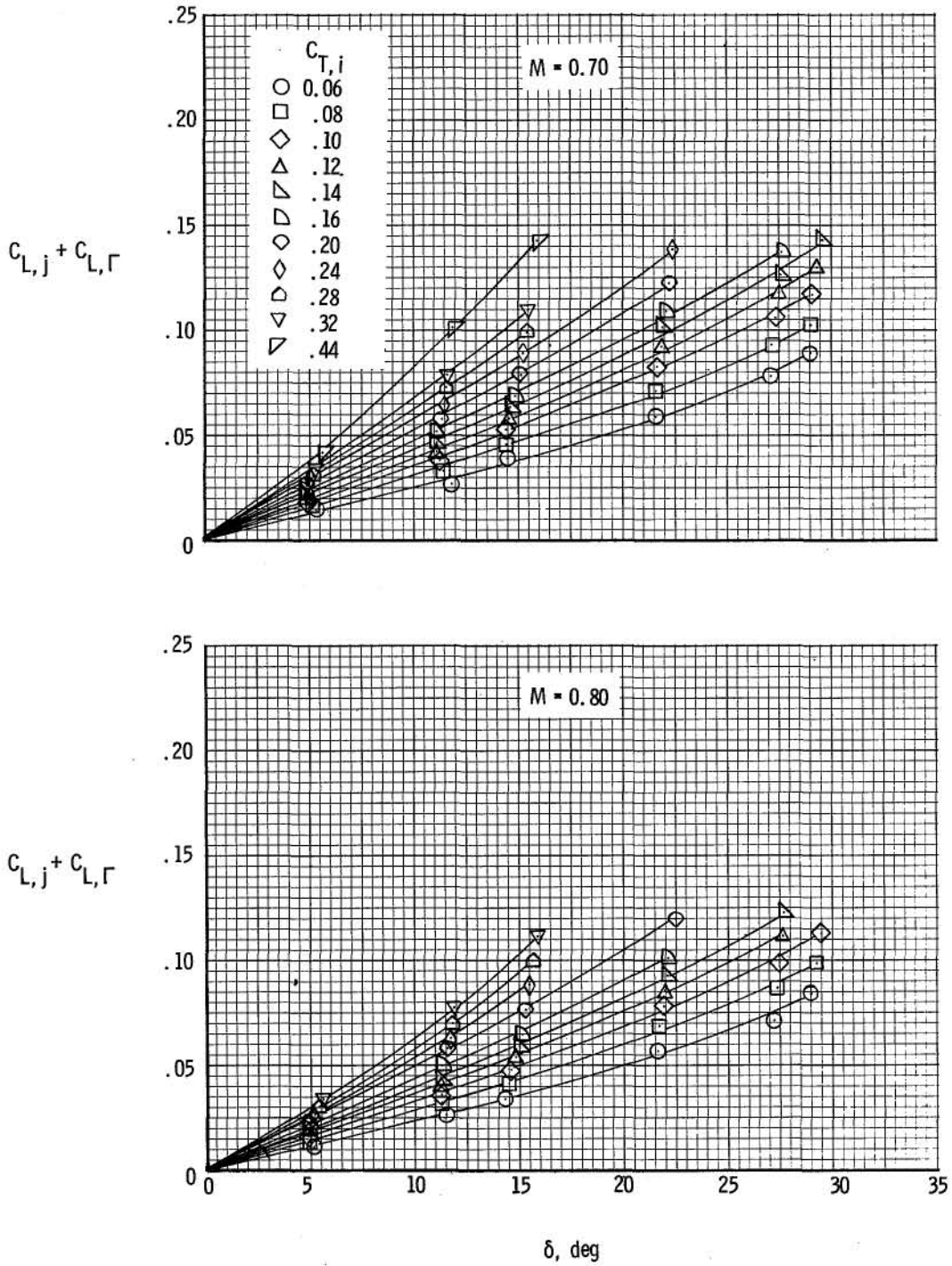

(b) M = 0.70 and 0.80.

Figure 9.- Continued.

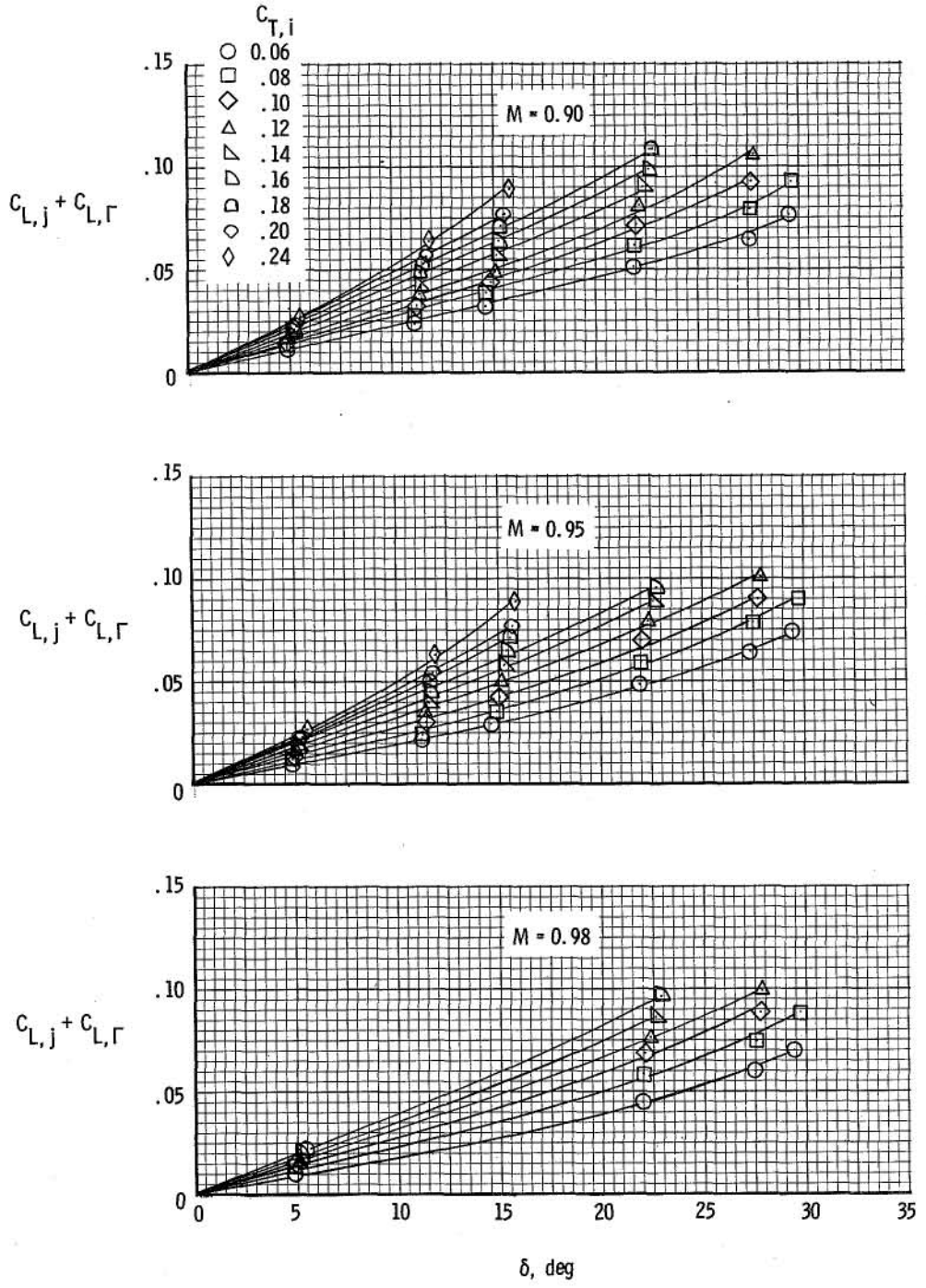

(c) M = 0.90, 0.95, and 0.98.

Figure 9.- Concluded.

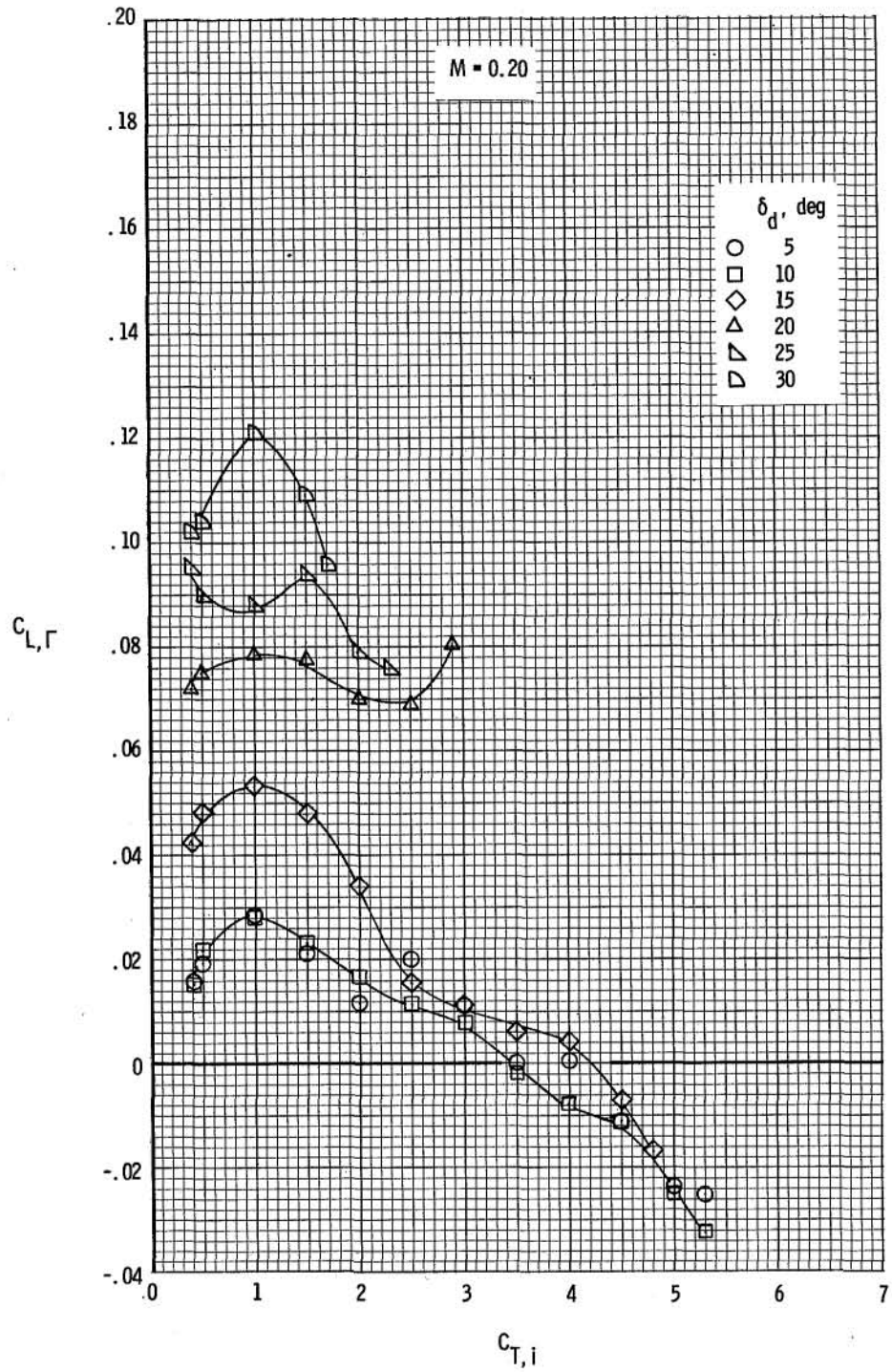

(a) M = 0.20.

Figure 10.- Variation of jet-circulation lift with ideal gross thrust coefficient for various exhaust-nozzle deflection angles. $i_w = -1.38^o$.

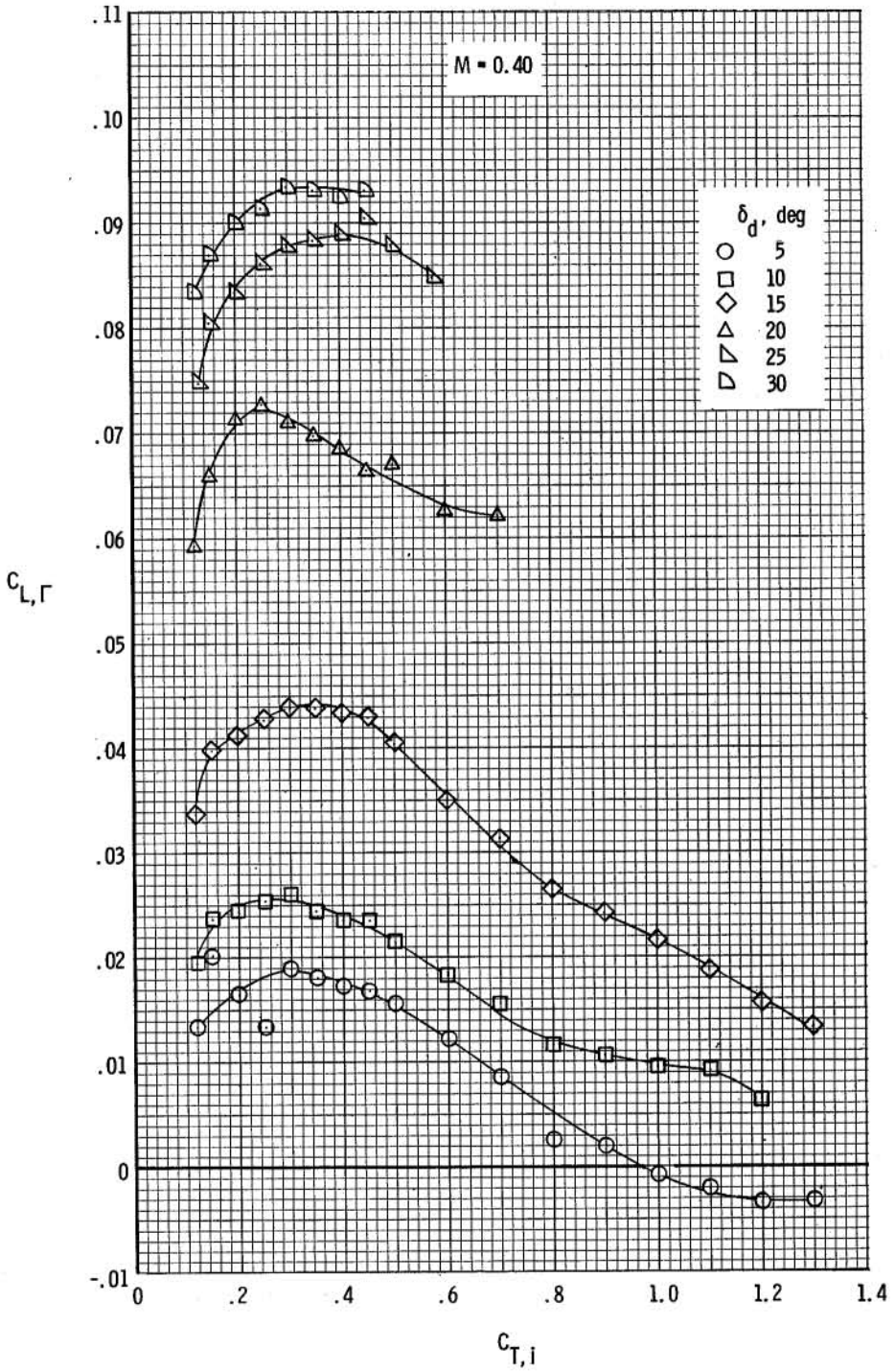

(b) M = 0.40.

Figure 10.- Continued.

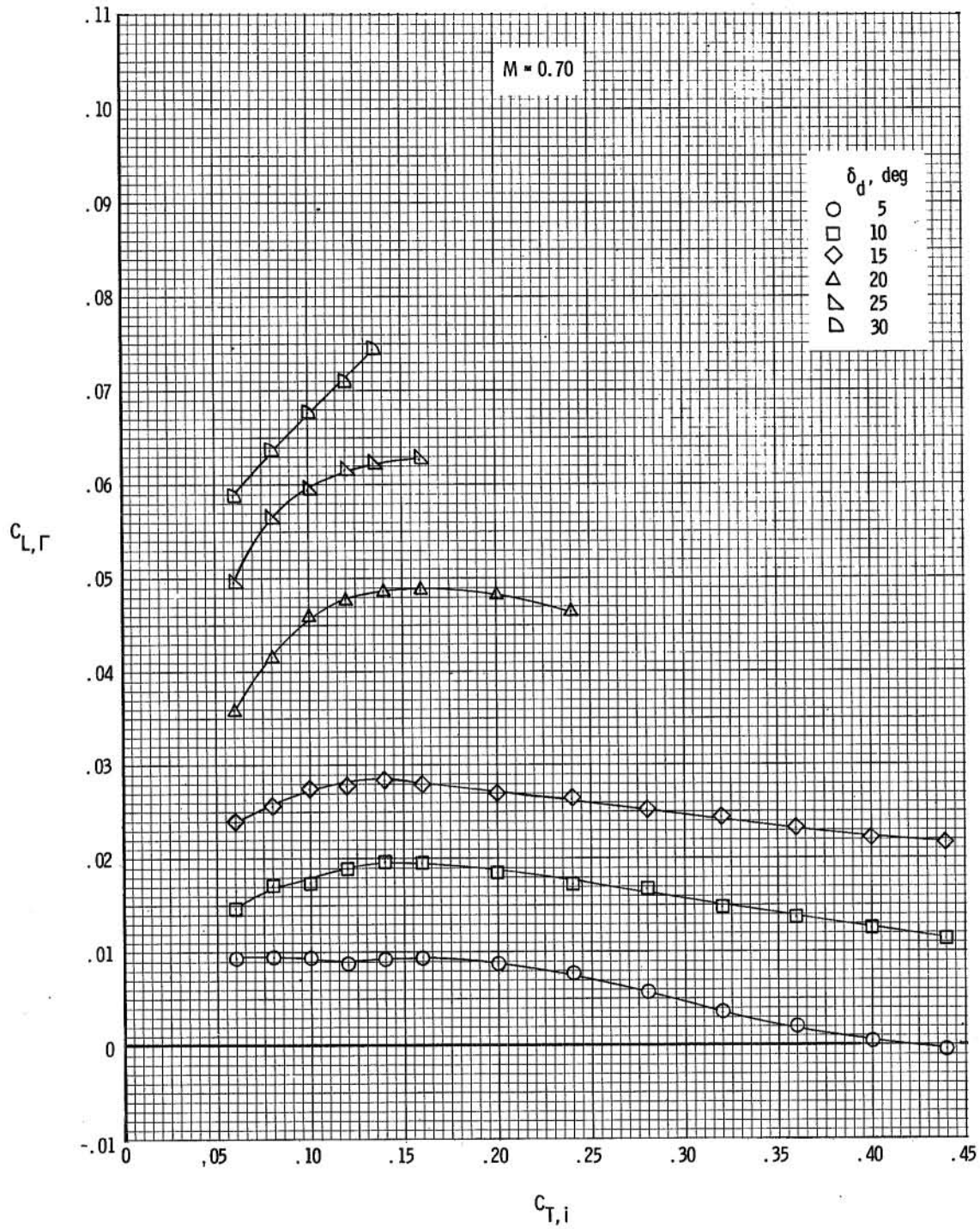

(c) M = 0.70.

Figure 10.- Continued.

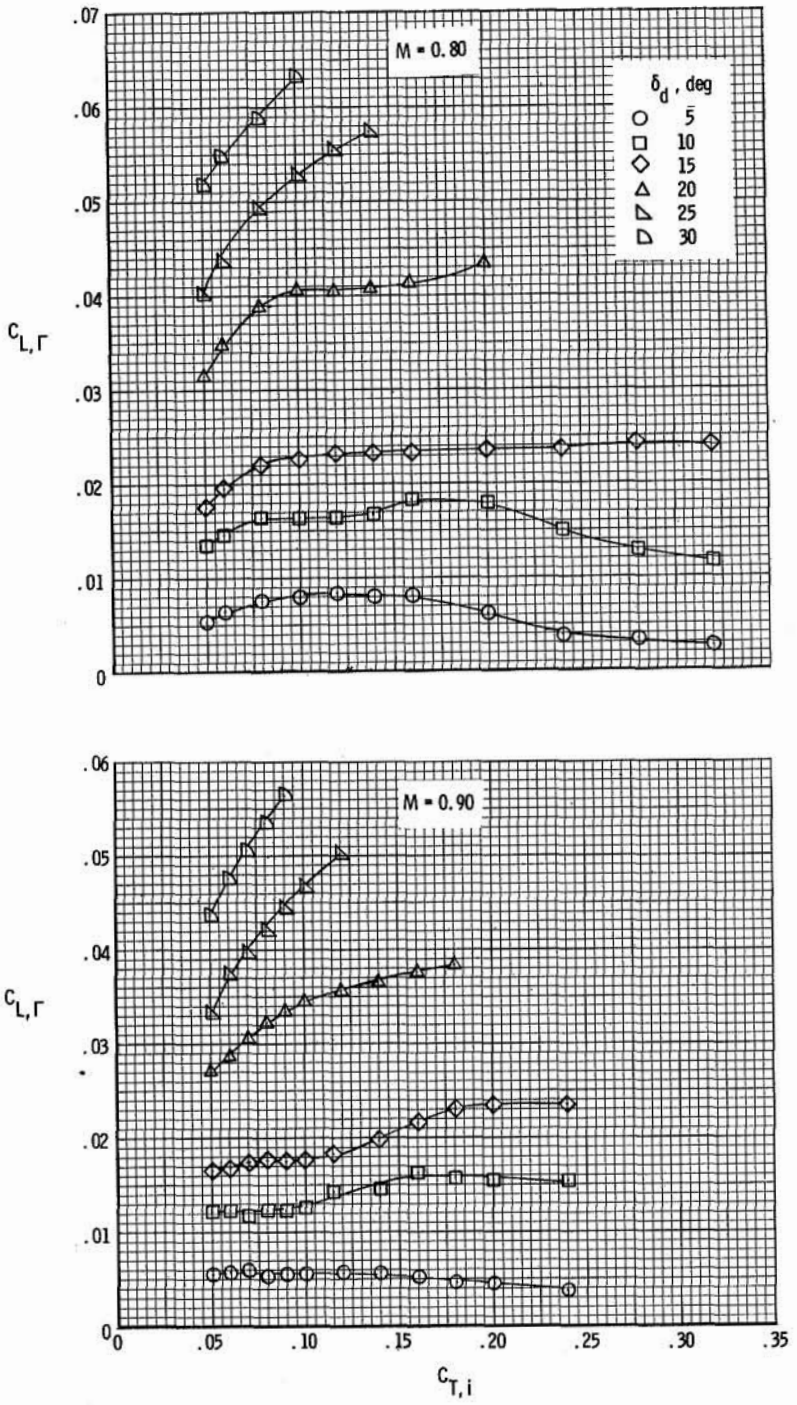

(d) M = 0.80 and 0.90.

Figure 10.- Continued.

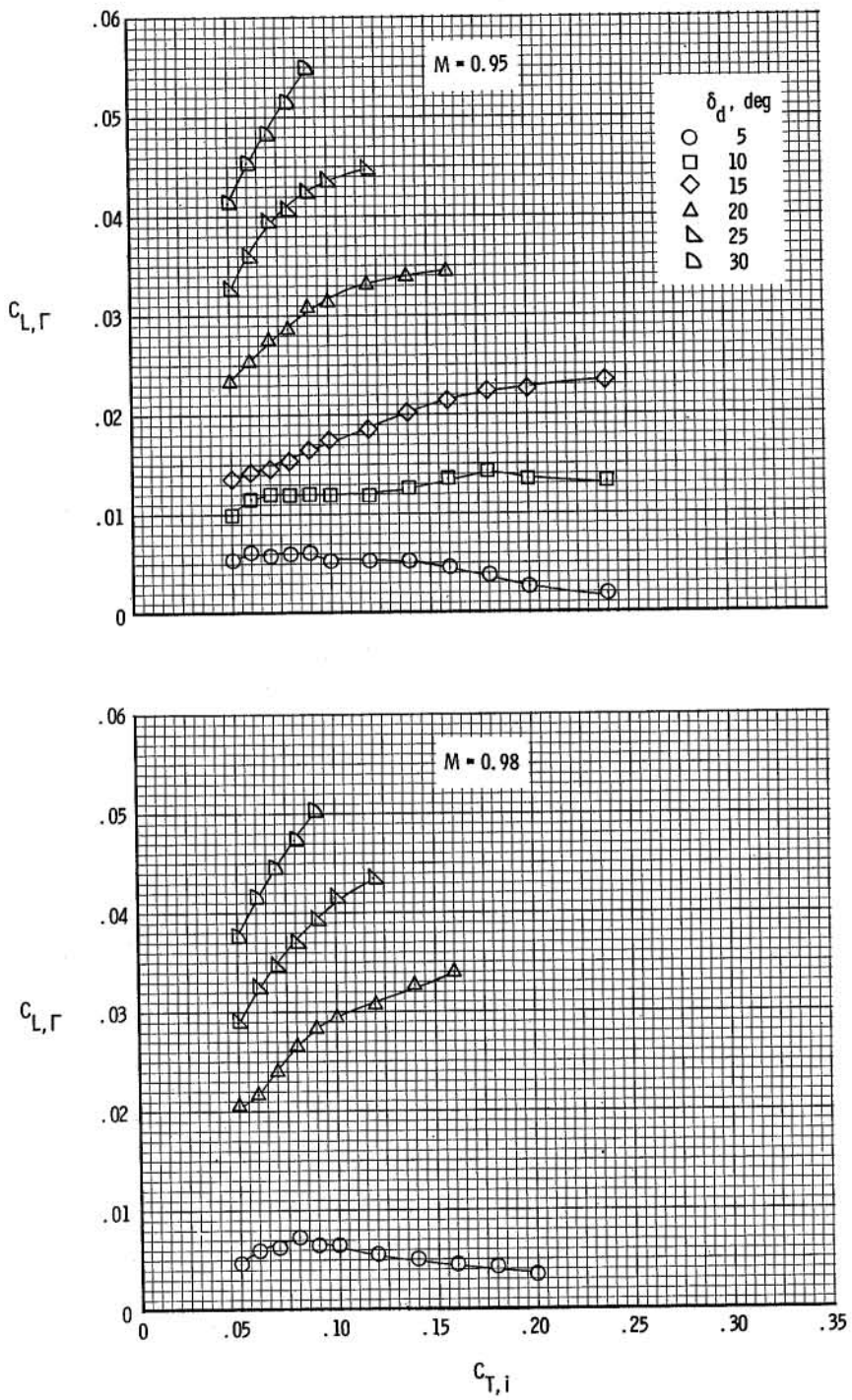

(e) M = 0.95 and 0.98.

Figure 10.- Concluded.

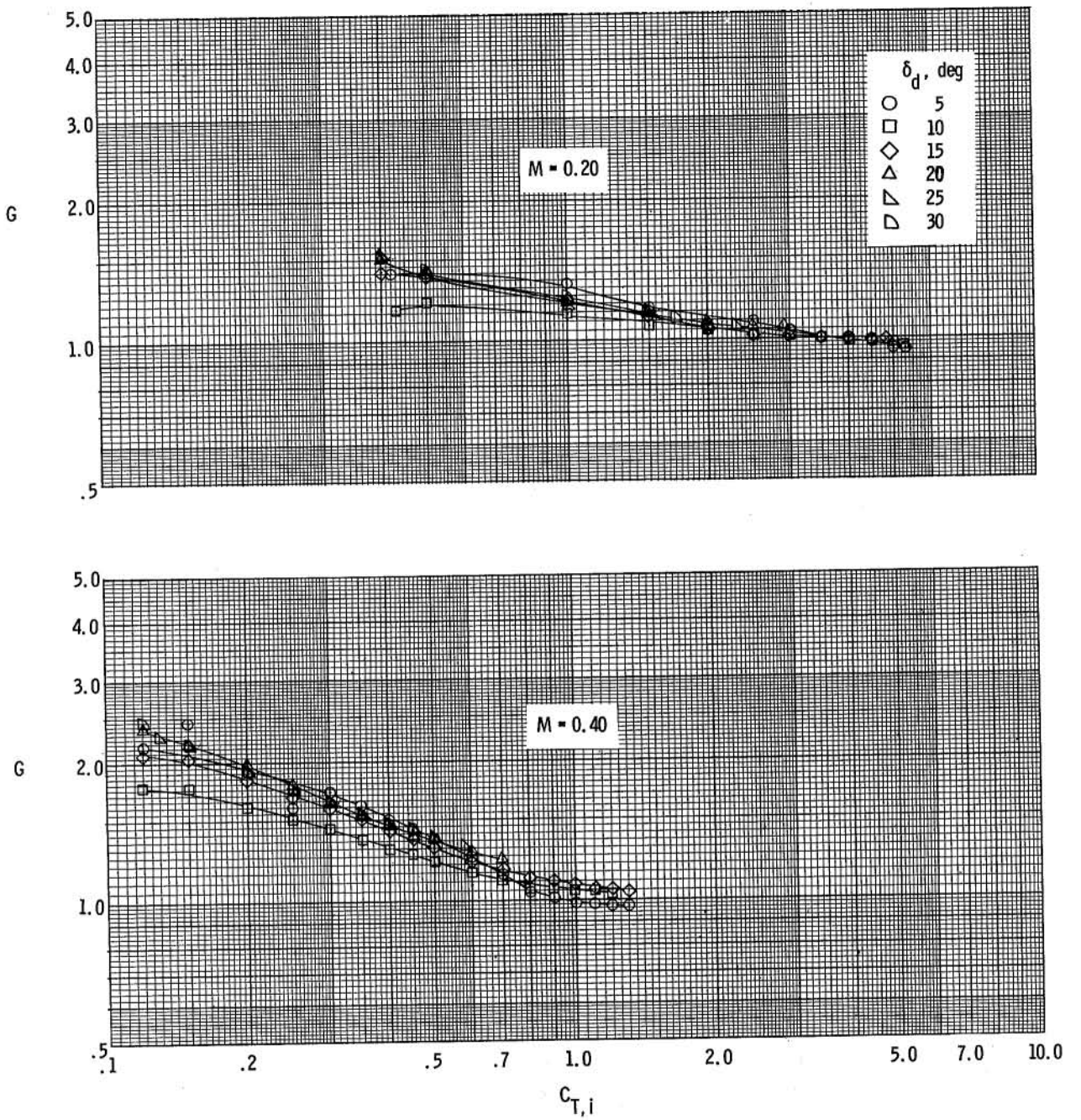

(a) M = 0.20 and 0.40.

Figure 11.- Variation of gain factor with ideal gross thrust coefficient for various exhaust-nozzle deflection angles. $i_w = -1.38^o$.

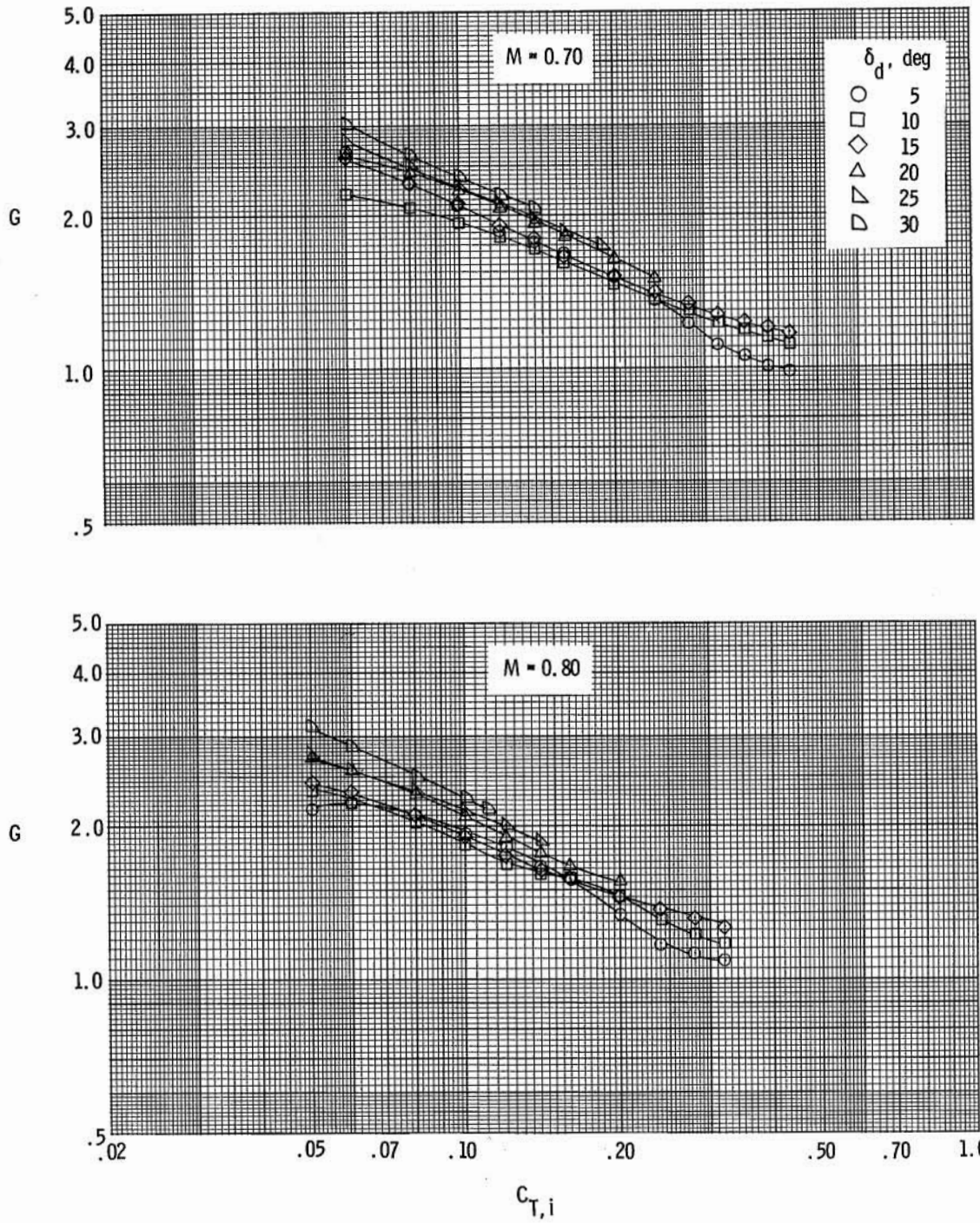

(b) M = 0.70 and 0.80.

Figure 11.- Continued.

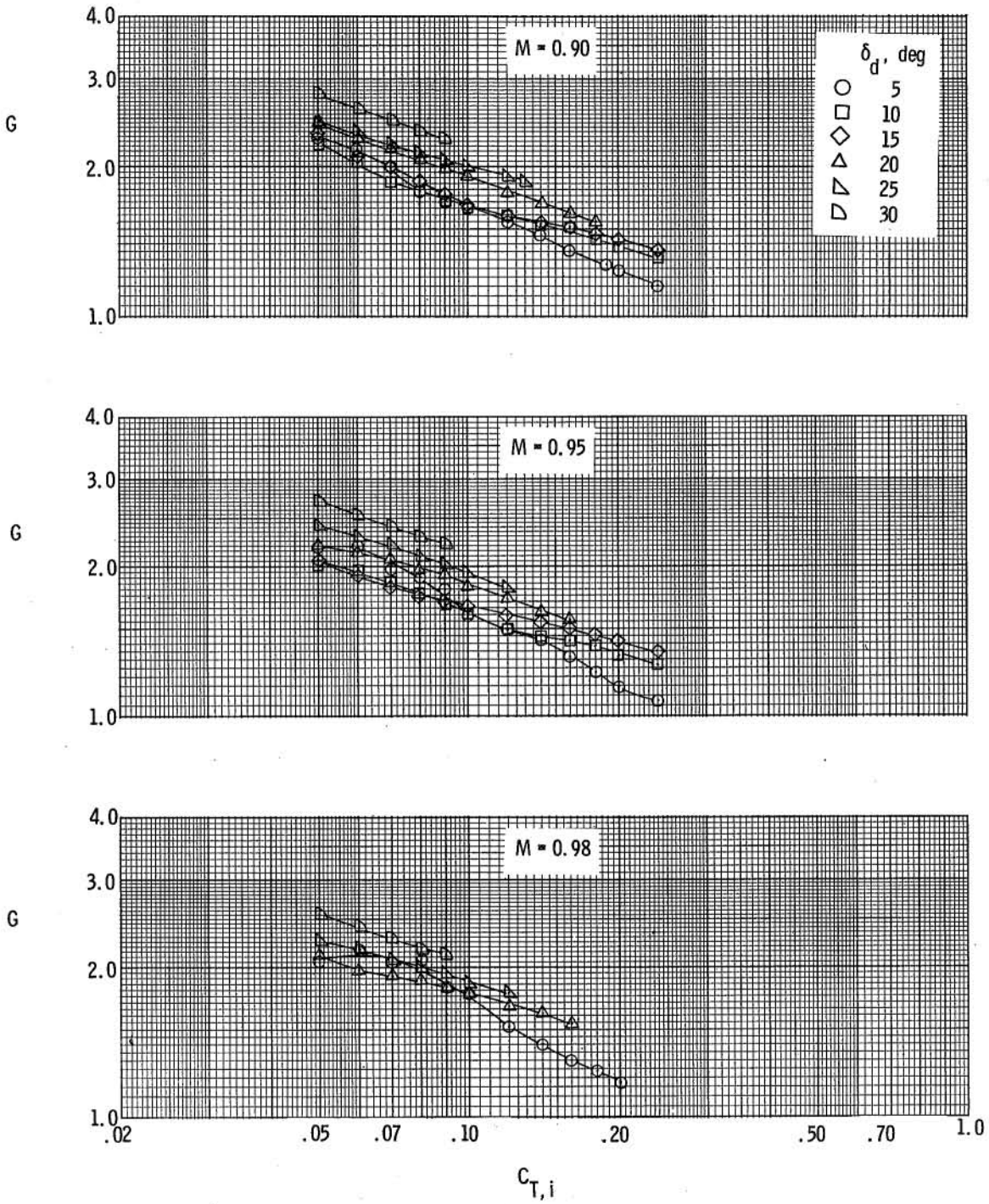

(c) M = 0.90, 0.95, and 0.98.

Figure 11.- Concluded.

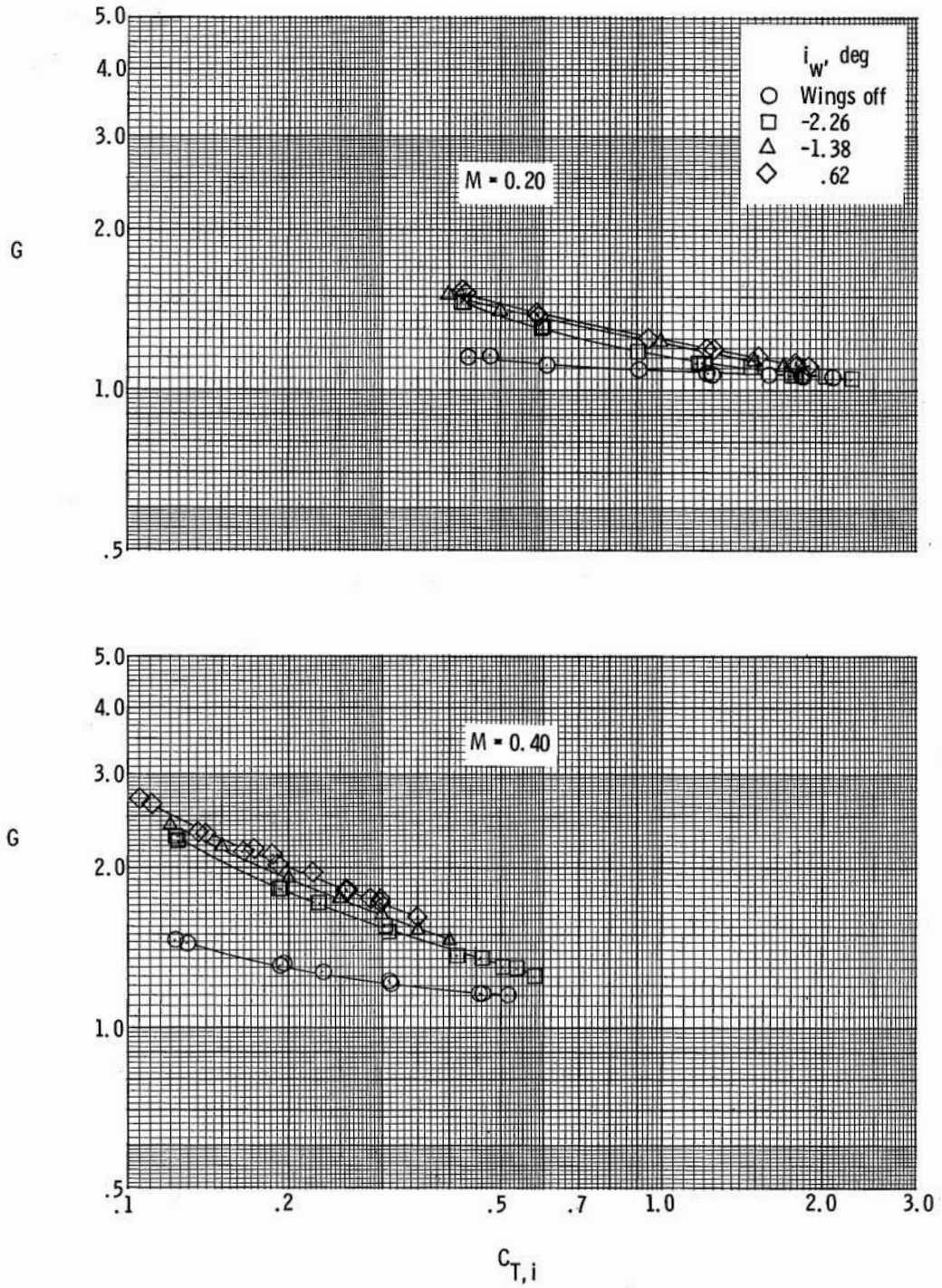

(a) M = 0.20 and 0.40.

Figure 12.- Effect of wings off and wing incidence angle on gain factor for exhaust nozzle with $\delta_d = 30^o$.

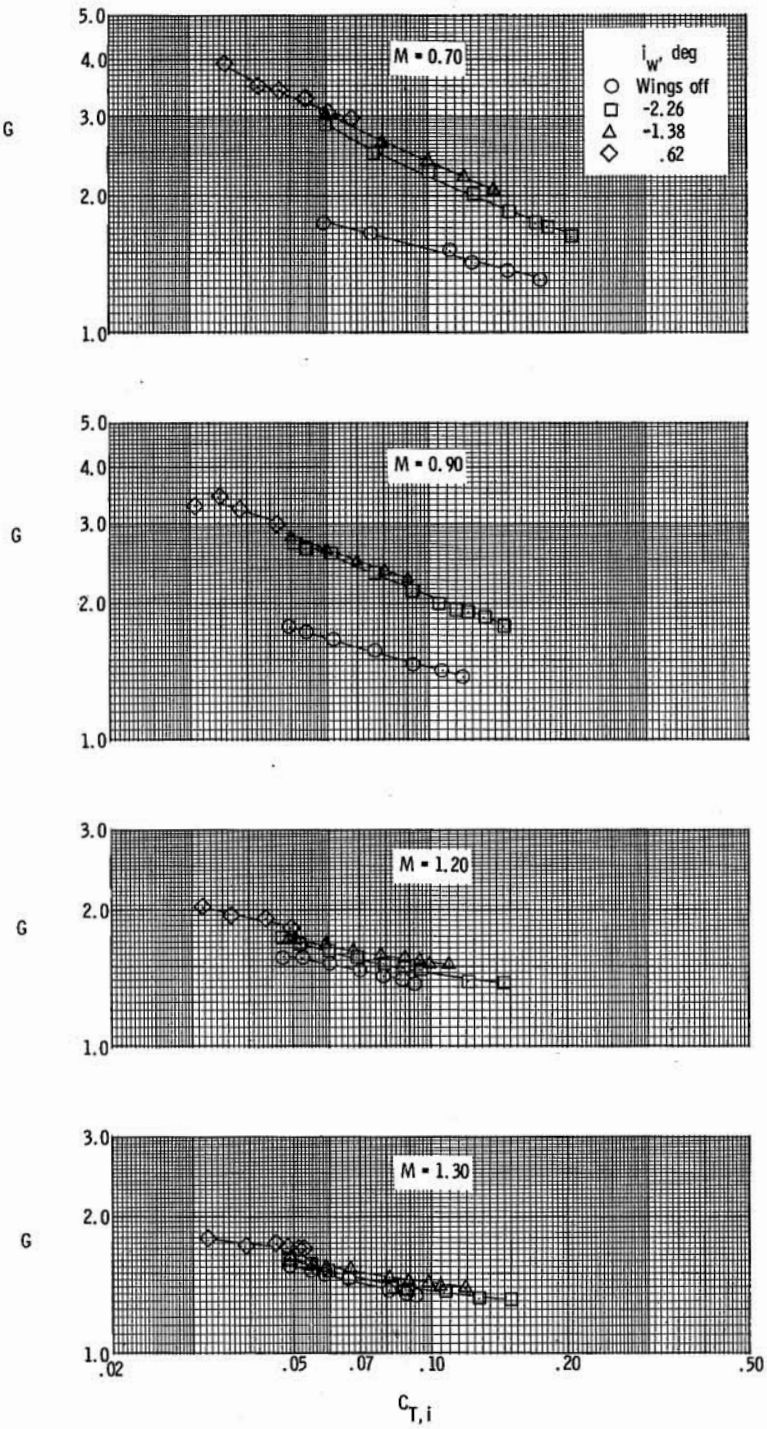

(b) M = 0.70, 0.90, 1.20, and 1.30.

Figure 12.- Concluded.

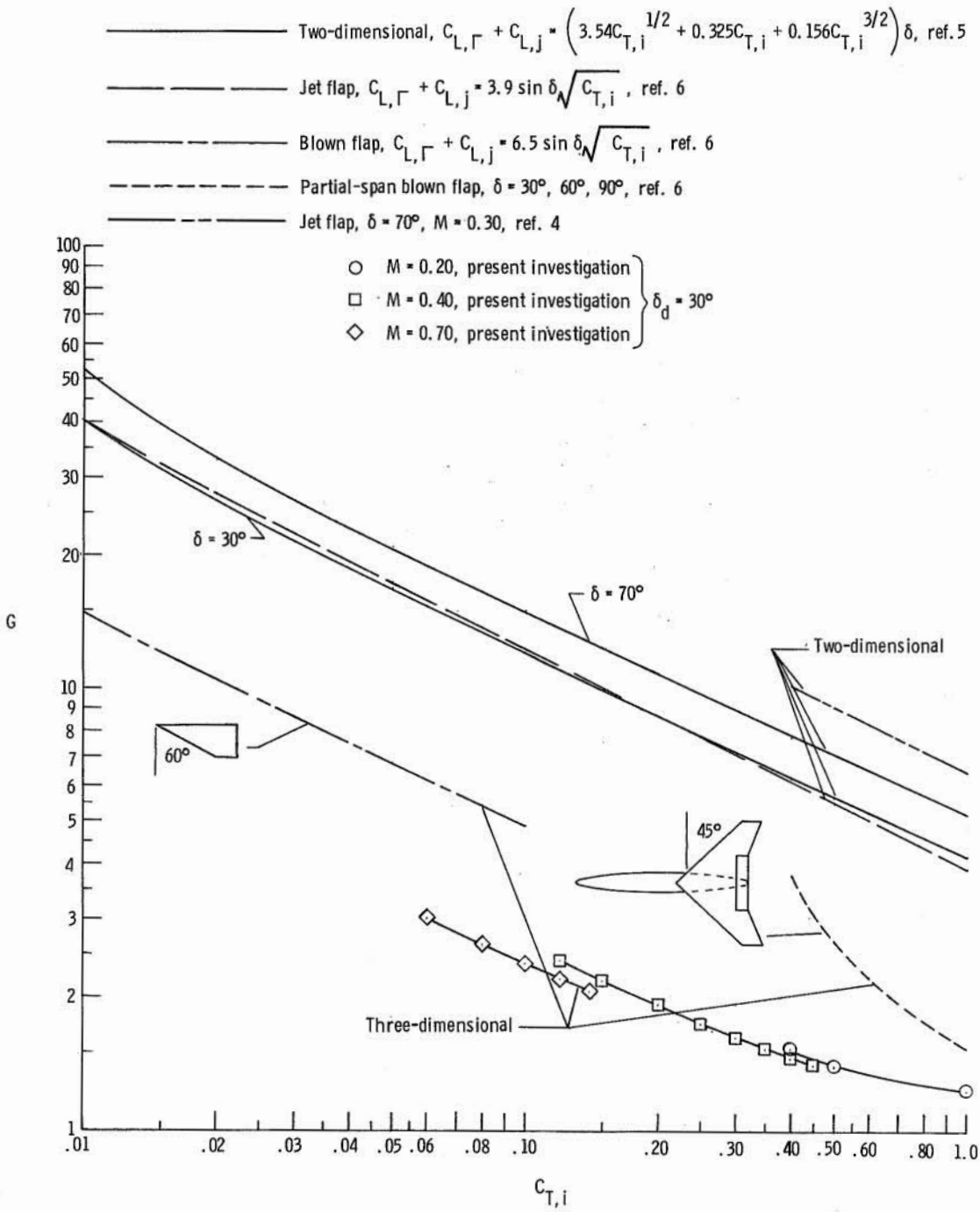

Figure 13.- Comparison of gain factors of present investigation with theoretical data and other experimental data.

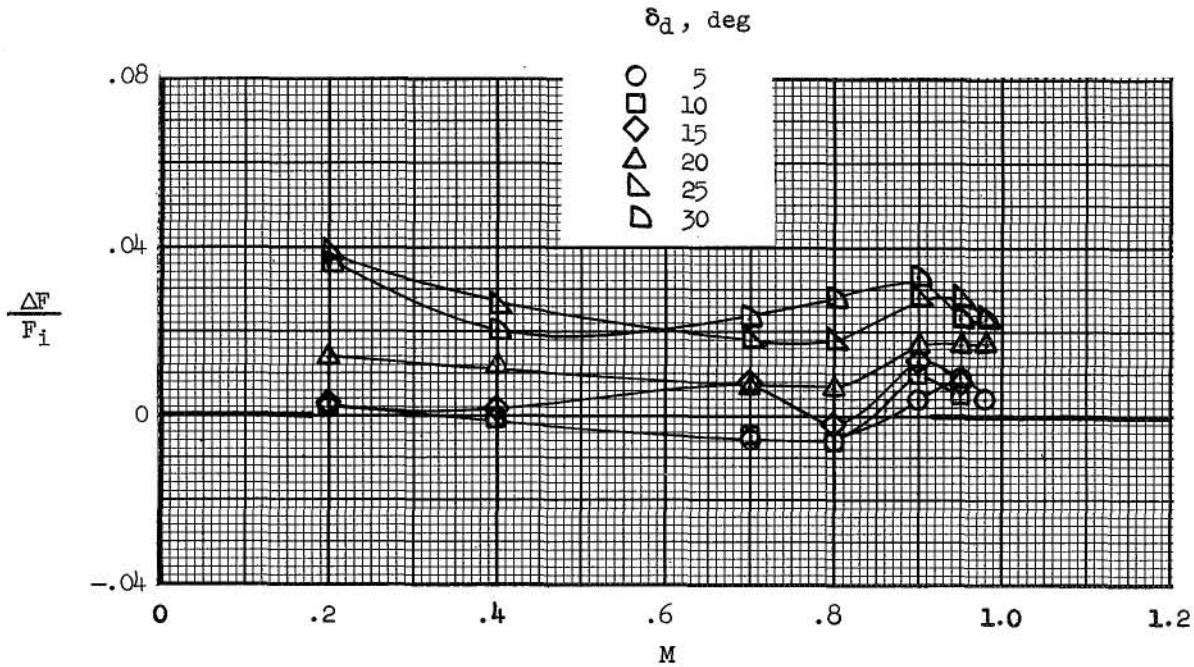

Figure 14.- Variation of thrust recovery parameter with Mach number for various exhaust-nozzle deflection angles. $i_w = -1.38^o$.

NATIONAL AERONAUTICS AND SPACE ADMINISTRATION
WASHINGTON, D.C. 20546

OFFICIAL BUSINESS
PENALTY FOR PRIVATE USE $300

FIRST CLASS MAIL

POSTAGE AND FEES PAID
NATIONAL AERONAUTICS AND
SPACE ADMINISTRATION

POSTMASTER: If Undeliverable (Section 158 Postal Manual) Do Not Return

"The aeronautical and space activities of the United States shall be conducted so as to contribute . . . to the expansion of human knowledge of phenomena in the atmosphere and space. The Administration shall provide for the widest practicable and appropriate dissemination of information concerning its activities and the results thereof."

—NATIONAL AERONAUTICS AND SPACE ACT OF 1958

NASA SCIENTIFIC AND TECHNICAL PUBLICATIONS

TECHNICAL REPORTS: Scientific and technical information considered important, complete, and a lasting contribution to existing knowledge.

TECHNICAL NOTES: Information less broad in scope but nevertheless of importance as a contribution to existing knowledge.

TECHNICAL MEMORANDUMS: Information receiving limited distribution because of preliminary data, security classification, or other reasons.

CONTRACTOR REPORTS: Scientific and technical information generated under a NASA contract or grant and considered an important contribution to existing knowledge.

TECHNICAL TRANSLATIONS: Information published in a foreign language considered to merit NASA distribution in English.

SPECIAL PUBLICATIONS: Information derived from or of value to NASA activities. Publications include conference proceedings, monographs, data compilations, handbooks, sourcebooks, and special bibliographies.

TECHNOLOGY UTILIZATION PUBLICATIONS: Information on technology used by NASA that may be of particular interest in commercial and other non-aerospace applications. Publications include Tech Briefs, Technology Utilization Reports and Technology Surveys.

Details on the availability of these publications may be obtained from:

SCIENTIFIC AND TECHNICAL INFORMATION OFFICE

NATIONAL AERONAUTICS AND SPACE ADMINISTRATION

Washington, D.C. 20546